J. Fluid Mech. (2017), *vol.* 824, *pp.* 286–311.
doi:10.1017/jfm.2017.343

Internal wave resonant triads in finite-depth non-uniform stratifications

Dheeraj Varma[1] **and Manikandan Mathur**[1,†]

[1]Department of Aerospace Engineering, Indian Institute of Technology Madras, Chennai - 600036, India

(Received 10 June 2016; revised 30 March 2017; accepted 17 May 2017;
first published online 5 July 2017)

We present a theoretical study of nonlinear effects that result from modal interactions in internal waves in a non-uniformly stratified finite-depth fluid with background rotation. A linear wave field containing modes m and n (of horizontal wavenumbers k_m and k_n) at a fixed frequency ω results in two different terms in the steady-state weakly nonlinear solution: (i) a superharmonic wave of frequency 2ω, horizontal wavenumber $k_m + k_n$ and a vertical structure $\bar{h}_{mn}(z)$ and (ii) a time-independent term (Eulerian mean flow) with horizontal wavenumber $k_m - k_n$. For some (m, n), $\bar{h}_{mn}(z)$ is infinitely large along specific curves on the $(\omega/N_0, f/\omega)$ plane, where N_0 and f are the deep ocean stratification and the Coriolis frequency, respectively; these curves are referred to as divergence curves in the rest of this paper. In uniform stratifications, a unique divergence curve occurs on the $(\omega/N_0, f/\omega)$ plane for those $(m, n \neq m)$ that satisfy $(m/3) < n < (3m)$. In the presence of a pycnocline (whose strength is quantified by the maximum stratification N_{max}), divergence curves occur for several more modal interactions than those for a uniform stratification; furthermore, a given (m, n) interaction can result in multiple divergence curves on the $(\omega/N_0, f/\omega)$ plane for a fixed N_{max}/N_0. Nearby high-mode interactions in a uniform stratification and any modal interaction in a non-uniform stratification with a sufficiently strong pycnocline are shown to result in near-horizontal divergence curves around $f/\omega \approx 1$, thus implying that strong nonlinear effects often occur as a result of interaction within triads containing two different modes at the near-inertial frequency. Notably, self-interaction of certain modes in a non-uniform stratification results in one or more divergence curves on the $(\omega/N_0, f/\omega)$ plane, thus suggesting that even arbitrarily small-amplitude individual modes cannot remain linear in a non-uniform stratification. We show that internal wave resonant triads containing modes m and n at frequency ω occur along the divergence curves, and their existence is guaranteed upon the satisfaction of two different criteria: (i) the horizontal component of the standard triadic resonance criterion $\boldsymbol{k}_1 + \boldsymbol{k}_2 + \boldsymbol{k}_3 = 0$ and (ii) a non-orthogonality criterion. For uniform stratifications, criterion (ii) reduces to the vertical component of the standard triadic resonance criterion. For non-uniform stratifications, criterion (ii) seems to be always satisfied whenever criterion (i) is satisfied, thus significantly increasing the number of modal interactions that result in strong nonlinear effects irrespective of the wave amplitudes. We then adapt our theoretical framework to identify resonant triads and hence provide insights into the generation of higher harmonics in two different oceanic scenarios: (i) low-mode internal tide propagating over small- or large-scale topography and (ii) an internal wave beam incident on a pycnocline in the upper

† Email address for correspondence: manims@ae.iitm.ac.in

ocean, for which our results are in qualitative agreement with the numerical study of Diamessis *et al.* (*Dynam. Atmos. Oceans.*, vol. 66, 2014, pp. 110–137).

Key words: internal waves, stratified flows, waves in rotating fluids

1. Introduction

Pathways of energy dissipation in internal waves generated by tides and winds are an important piece in the puzzle of understanding vertical mixing and the global energy budget in the ocean (Munk & Wunsch 1998). In this paper, we study a nonlinear mechanism of superharmonic wave generation as a result of interaction between various vertical modes of internal waves at a fixed frequency.

Linear internal wave fields in the finite-depth ocean are conveniently represented using vertical modes, which ensures that the boundary conditions on the ocean floor and the free surface (often modelled as a rigid lid) are satisfied (Gill 1982). Internal tide generation arising from barotropic tidal flow over bottom topography is understood to result in a range of vertical modes at the semidiurnal frequency, with the high modes getting dissipated near the generation sites and the low modes travelling far (Garrett & Kunze 2007). Subsequent processes such as scattering by short or tall deep ocean topography and continental shelves further transfer energy from the far-travelling low modes to higher modes at the same frequency (Johnston, Merrifield & Holloway 2003; Klymak *et al.* 2011; Mathur, Carter & Peacock 2014). Similarly, the spatially compact near-inertial currents excited in the mixed layer by surface winds generate a whole range of high modes, with a modal representation and the calculation of the evolution of the modal amplitudes providing insight into the mechanisms by which near-inertial waves propagate into the deep ocean (D'Asaro 1989; Balmforth & Young 1999). While the transfer of energy to higher modes, and hence shorter spatial scales, is generally recognized as conducive to instabilities and mixing, the exact mechanisms leading to internal wave energy dissipation are not well understood. The nonlinear effects that may result from the presence of a range of vertical modes at a given frequency in a non-uniform stratification are the focus of the current study.

One of the well-known instability mechanisms in internal waves is the resonant triad interaction (RTI) (Staquet & Sommeria 2002). In uniformly stratified fluid of infinite horizontal and vertical extents, three interacting internal waves satisfying the relations $\omega_1 + \omega_2 + \omega_3 = 0$ and $\boldsymbol{k}_1 + \boldsymbol{k}_2 + \boldsymbol{k}_3 = 0$ form a resonant triad, where $\boldsymbol{k}_{1,2,3}$ are the wave vectors and $\omega_{1,2,3}$ are the corresponding frequencies (positive or negative) obtained from the linear internal wave dispersion relation (Hasselmann 1967; LeBlond & Mysak 1981). In arbitrary non-uniform stratifications, however, there exists no such simple analytical criterion for a pure resonant wave triad. In this paper, we show that pure resonant triads exist in a finite-depth non-uniform stratification, and we also identify the conditions for the same.

An important consequence of RTI is the parametric subharmonic instability (PSI), where a primary plane internal wave (above a threshold amplitude) at frequency ω_0 in a viscous, uniformly stratified fluid results in the growth of secondary waves that form a resonant triad with the primary wave (Koudella & Staquet 2006; Bourget *et al.* 2013). The secondary waves with the maximum growth rate occur at frequencies $\omega_{1,2} < \omega_0$, with the relation $\omega_1 \approx \omega_2 \approx \omega_0/2$ holding in the limit of relatively large

wavenumbers of the secondary waves (Staquet & Sommeria 2002). In an internal wave beam, constructed as a superposition of unidirectional plane waves at a fixed frequency, PSI is less likely to occur, with various studies highlighting the importance of incorporating the effect of the finite spatial extent of the wave beam (Clark & Sutherland 2010; Bourget *et al.* 2013; Karimi & Akylas 2014). PSI has been observed in experimental studies of propagating internal wave modes too, with the triads corresponding to large theoretical growth rates shown to emerge (Martin, Simmons & Wunsch 1972; Joubaud *et al.* 2012).

RTI can also result from the presence of two finite-amplitude primary waves. For example, interaction between reflecting or colliding wave beams at a fixed frequency ω results in the generation of higher harmonic wave beams at frequency 2ω (Peacock & Tabaei 2005; Tabaei, Akylas & Lamb 2005). The interaction between plane waves contained within a unidirectional wave beam at frequency ω, however, does not result in the generation of higher harmonics, as the unidirectional wave beam in a uniformly stratified fluid of an infinite extent is an exact solution of the nonlinear equations as well (Tabaei & Akylas 2003). In contrast, in a finite-depth fluid, any linear internal wave field is a superposition of modes, and hence not necessarily an exact solution to the nonlinear equations of motion. As shown by Thorpe (1966) for a uniform stratification with no background rotation, two primary internal wave modes at a fixed frequency can interact to form a resonant triad.

To the best of our knowledge, while the generation of subharmonic and superharmonic waves in non-uniform stratifications has been reported in field observations (Xie *et al.* 2013), theoretical studies (Thorpe 1998; Young, Tsang & Balmforth 2008; Wunsch 2015), laboratory experiments (Wunsch & Brandt 2012; Wunsch *et al.* 2015; Ghaemsaidi *et al.* 2016) and numerical simulations (Gayen & Sarkar 2013; Diamessis *et al.* 2014; Wunsch *et al.* 2014), no previous studies have rigorously defined and identified resonant triads arising from modal interactions in non-uniformly stratified finite-depth media. In this paper, we construct the steady-state weakly nonlinear solution that corresponds to the leading-order solution containing an arbitrary sum of vertical modes at a given frequency in non-uniformly stratified media with background rotation, and thereby identify resonant triads via the divergence of the weakly nonlinear solution. Section 2 discusses the theory, followed by the results in § 3. The relevance of our theoretical results to two different oceanic scenarios is presented in § 4, followed by the conclusions in § 5.

2. Theory

The nonlinear governing equations for two-dimensional, incompressible, inviscid internal waves on the f-plane under the Boussinesq approximation are (LeBlond & Mysak 1981)

$$\frac{\partial^2}{\partial t^2}(\nabla^2\psi)+f^2\frac{\partial^2\psi}{\partial z^2}=\frac{g}{\rho^*}\frac{\partial}{\partial x}[J(\psi,\rho)]-\frac{\partial}{\partial t}[J(\psi,\nabla^2\psi)]+f\frac{\partial}{\partial z}[J(\psi,v)], \tag{2.1}$$

$$\frac{\partial\rho}{\partial t}=-J(\psi,\rho), \tag{2.2}$$

$$\frac{\partial v}{\partial t}+J(\psi,v)=f\frac{\partial\psi}{\partial z}, \tag{2.3}$$

where x and z are the horizontal and vertical coordinates and t is time; $\psi(x, z, t)$, $v(x, z, t)$ and $\rho(x, z, t)$ are the streamfunction, y-component of velocity and density, respectively, with the velocity components in the (x, z) plane given by $(u, w) = (-\partial\psi/\partial z, \partial\psi/\partial x)$; ρ^* is a reference constant density, f the Coriolis frequency and g the acceleration due to gravity. The Jacobian operator J is defined as $J(A, B) = (\partial A/\partial x)(\partial B/\partial z) - (\partial B/\partial x)(\partial A/\partial z)$, and $\nabla^2 = \partial^2/\partial x^2 + \partial^2/\partial z^2$. A no-normal-flow boundary condition at the horizontal boundaries of the fluid of depth H is specified as $\psi(x, z = 0, t) = \psi(x, z = H, t) = 0$. We now proceed to perform a weakly nonlinear analysis, which is a well-established mathematical tool as is described in LeBlond & Mysak (1981).

In the framework of regular perturbation expansion, we seek solutions of the form

$$(\psi, v, \rho) = (\psi_0, v_0, \rho_0) + \epsilon(\psi_1, v_1, \rho_1) + \epsilon^2(\psi_2, v_2, \rho_2) + \cdots, \tag{2.4}$$

where the small parameter ϵ quantifies the relative magnitude of the nonlinear terms in the governing equations. Substituting the solution forms of (ψ, v, ρ) in (2.4) into (2.1)–(2.3), we obtain

$$\begin{aligned}
&\left[\frac{\partial^2}{\partial t^2}(\nabla^2\psi_0) + f^2\frac{\partial^2\psi_0}{\partial z^2}\right] + \epsilon\left[\frac{\partial^2}{\partial t^2}(\nabla^2\psi_1) + f^2\frac{\partial^2\psi_1}{\partial z^2}\right] + \epsilon^2\left[\frac{\partial^2}{\partial t^2}(\nabla^2\psi_2) + f^2\frac{\partial^2\psi_2}{\partial z^2}\right] \\
&\quad = \left[\frac{g}{\rho^*}\frac{\partial}{\partial x}[J(\psi_0, \rho_0)] - \frac{\partial}{\partial t}[J(\psi_0, \nabla^2\psi_0)] + f\frac{\partial}{\partial z}(J(\psi_0, v_0))\right] \\
&\qquad + \epsilon\left[\frac{g}{\rho^*}\frac{\partial}{\partial x}[J(\psi_0, \rho_1) + J(\psi_1, \rho_0)] - \frac{\partial}{\partial t}[J(\psi_0, \nabla^2\psi_1) + J(\psi_1, \nabla^2\psi_0)]\right. \\
&\qquad \left. + f\frac{\partial}{\partial z}[J(\psi_0, v_1) + J(\psi_1, v_0)]\right] + \epsilon^2\left[\frac{g}{\rho^*}\frac{\partial}{\partial x}[J(\psi_0, \rho_2) + J(\psi_1, \rho_1) + J(\psi_2, \rho_0)]\right. \\
&\qquad - \frac{\partial}{\partial t}[J(\psi_0, \nabla^2\psi_2) + J(\psi_1, \nabla^2\psi_1) + J(\psi_2, \nabla^2\psi_0)] \\
&\qquad \left. + f\frac{\partial}{\partial z}[J(\psi_0, v_2) + J(\psi_1, v_1) + J(\psi_2, v_0)]\right]
\end{aligned} \tag{2.5}$$

$$\begin{aligned}
\frac{\partial\rho_0}{\partial t} + \epsilon\left[\frac{\partial\rho_1}{\partial t}\right] + \epsilon^2\left[\frac{\partial\rho_2}{\partial t}\right] &= -J(\psi_0, \rho_0) - \epsilon[J(\psi_0, \rho_1) + J(\psi_1, \rho_0)] \\
&\quad - \epsilon^2[J(\psi_0, \rho_2) + J(\psi_1, \rho_1) + J(\psi_2, \rho_0)],
\end{aligned} \tag{2.6}$$

$$\begin{aligned}
&\frac{\partial v_0}{\partial t} + J(\psi_0, v_0) + \epsilon\left[\frac{\partial v_1}{\partial t} + J(\psi_0, v_1) + J(\psi_1, v_0)\right] \\
&\qquad + \epsilon^2\left[\frac{\partial v_2}{\partial t} + J(\psi_0, v_2) + J(\psi_1, v_1) + J(\psi_2, v_0)\right] \\
&\quad = f\frac{\partial\psi_0}{\partial z} + \epsilon f\frac{\partial\psi_1}{\partial z} + \epsilon^2 f\frac{\partial\psi_2}{\partial z}.
\end{aligned} \tag{2.7}$$

The solution at $O(\epsilon^0)$ is assumed as $\psi_0 = 0$, $v_0 = 0$ and $\rho_0 = \bar{\rho}(z)$ with the stratification profile $N(z) = \sqrt{(-g/\rho^*)\,\mathrm{d}\bar{\rho}/\mathrm{d}z}$. In other words, the background flow is described by a static, stably stratified fluid.

Substituting (ψ_0, ρ_0, v_0) into (2.5)–(2.7) and retaining only the $O(\epsilon)$ terms, we obtain the governing equations for (ψ_1, ρ_1, v_1) as

$$\frac{\partial^2}{\partial t^2}(\nabla^2\psi_1) + f^2\frac{\partial^2\psi_1}{\partial z^2} + N^2\frac{\partial^2\psi_1}{\partial x^2} = 0, \tag{2.8}$$

$$\frac{\partial\rho_1}{\partial t} = \frac{\rho^*}{g}N^2\frac{\partial\psi_1}{\partial x}, \tag{2.9}$$

$$\frac{\partial v_1}{\partial t} = f\frac{\partial\psi_1}{\partial z}, \tag{2.10}$$

with ψ_1 satisfying the boundary conditions $\psi_1(z=0) = \psi_1(z=H) = 0$. We assume (ψ_1, ρ_1, v_1) to be described by a superposition of right-propagating linear internal wave modes (LeBlond & Mysak 1981) at a given frequency $\omega > 0$ and write

$$\psi_1 = \sum_{n=1}^{\infty}\sqrt{\frac{2\omega k_n E_n}{\rho^*(\omega^2 - f^2)\displaystyle\int_0^H\left(\frac{\mathrm{d}\Phi_n}{\mathrm{d}z}\right)^2\mathrm{d}z}}\,\Phi_n(z)\cos(k_n x - \omega t + \alpha_n), \tag{2.11}$$

where the mode shape $\Phi_n(z)$ and horizontal wavenumber $k_n > 0$ satisfy

$$\frac{\mathrm{d}^2\Phi_n}{\mathrm{d}z^2} + \frac{k_n^2(N^2 - \omega^2)}{\omega^2 - f^2}\Phi_n = 0. \tag{2.12}$$

In (2.11), E_n is the vertically averaged horizontal energy flux in the nth mode. The energy flux E_n is assumed to be independent of time, thus implying that we are constructing a steady-state weakly nonlinear solution. Corresponding solutions to the equations in (2.9) and (2.10) are

$$\rho_1 = \frac{1}{\omega}\frac{\mathrm{d}\rho_0}{\mathrm{d}z}\sum_{n=1}^{\infty}\sqrt{\frac{2\omega k_n E_n}{\rho^*(\omega^2 - f^2)\displaystyle\int_0^H\left(\frac{\mathrm{d}\Phi_n}{\mathrm{d}z}\right)^2\mathrm{d}z}}\,k_n\Phi_n(z)\cos(k_n x - \omega t + \alpha_n), \tag{2.13}$$

$$v_1 = \frac{-f}{\omega}\sum_{n=1}^{\infty}\sqrt{\frac{2\omega k_n E_n}{\rho^*(\omega^2 - f^2)\displaystyle\int_0^H\left(\frac{\mathrm{d}\Phi_n}{\mathrm{d}z}\right)^2\mathrm{d}z}}\,\frac{\mathrm{d}\Phi_n}{\mathrm{d}z}\sin(k_n x - \omega t + \alpha_n). \tag{2.14}$$

Substituting (ψ_0, ρ_0, v_0) into (2.5), the $O(\epsilon^2)$ terms generate the governing equation for ψ_2 as

$$\frac{\partial^2}{\partial t^2}(\nabla^2\psi_2) + f^2\frac{\partial^2\psi_2}{\partial z^2} + N^2\frac{\partial^2\psi_2}{\partial x^2} = \frac{g}{\rho^*}\frac{\partial}{\partial x}[J(\psi_1, \rho_1)] - \frac{\partial}{\partial t}[J(\psi_1, \nabla^2\psi_1)] + f\frac{\partial}{\partial z}[J(\psi_1, v_1)]. \tag{2.15}$$

The right-hand side of (2.15), which we denote by R, is evaluated by substituting the solutions for (ψ_1, ρ_1, v_1) from expressions (2.11), (2.13) and (2.14) to give

$$\left.\begin{aligned}
R = &\sum_{m=1}^{\infty}\sum_{n=1}^{\infty}[A_{mn}\cos((k_m+k_n)x-2\omega t+\alpha_m+\alpha_n)\\
&+B_{mn}\cos((k_m-k_n)x+\alpha_m-\alpha_n)],\\
A_{mn}(z) = &\frac{2\omega}{\rho^*(\omega^2-f^2)}\sqrt{\frac{k_mk_nE_mE_n}{\displaystyle\int_0^H\left(\frac{\mathrm{d}\Phi_m}{\mathrm{d}z}\right)^2\mathrm{d}z\int_0^H\left(\frac{\mathrm{d}\Phi_n}{\mathrm{d}z}\right)^2\mathrm{d}z}}\\
&\times\left(\frac{\Phi_mk_mk_n}{2\omega}\left[N^2\frac{\mathrm{d}\Phi_n}{\mathrm{d}z}+\frac{\mathrm{d}(N^2)}{\mathrm{d}z}\Phi_n\right](k_m+k_n)-\frac{\Phi_nk_n^2}{2\omega}\frac{\mathrm{d}\Phi_m}{\mathrm{d}z}N^2(k_m+k_n)\right.\\
&-\omega\left[\Phi_mk_m\left(\frac{\mathrm{d}^3\Phi_n}{\mathrm{d}z^3}-k_n^2\frac{\mathrm{d}\Phi_n}{\mathrm{d}z}\right)-\frac{\mathrm{d}\Phi_m}{\mathrm{d}z}k_n\left(\frac{\mathrm{d}^2\Phi_n}{\mathrm{d}z^2}-k_n^2\Phi_n\right)\right]\\
&\left.-\frac{f^2}{2\omega}\left[k_m\frac{\mathrm{d}\Phi_m}{\mathrm{d}z}\frac{\mathrm{d}^2\Phi_n}{\mathrm{d}z^2}+k_m\Phi_m\frac{\mathrm{d}^3\Phi_n}{\mathrm{d}z^3}-k_n\frac{\mathrm{d}^2\Phi_m}{\mathrm{d}z^2}\frac{\mathrm{d}\Phi_n}{\mathrm{d}z}-k_n\frac{\mathrm{d}^2\Phi_n}{\mathrm{d}z^2}\frac{\mathrm{d}\Phi_m}{\mathrm{d}z}\right]\right),\\
B_{mn}(z) = &\frac{2\omega}{\rho^*(\omega^2-f^2)}\sqrt{\frac{k_mk_nE_mE_n}{\displaystyle\int_0^H\left(\frac{\mathrm{d}\Phi_m}{\mathrm{d}z}\right)^2\mathrm{d}z\int_0^H\left(\frac{\mathrm{d}\Phi_n}{\mathrm{d}z}\right)^2\mathrm{d}z}}\\
&\times\left(\frac{\Phi_mk_mk_n}{2\omega}\left[N^2\frac{\mathrm{d}\Phi_n}{\mathrm{d}z}+\frac{\mathrm{d}(N^2)}{\mathrm{d}z}\Phi_n\right](k_m-k_n)+\frac{\Phi_nk_n^2}{2\omega}\frac{\mathrm{d}\Phi_m}{\mathrm{d}z}N^2(k_m-k_n)\right.\\
&\left.+\frac{f^2}{2\omega}\left[k_m\frac{\mathrm{d}\Phi_m}{\mathrm{d}z}\frac{\mathrm{d}^2\Phi_n}{\mathrm{d}z^2}+k_m\Phi_m\frac{\mathrm{d}^3\Phi_n}{\mathrm{d}z^3}+k_n\frac{\mathrm{d}^2\Phi_m}{\mathrm{d}z^2}\frac{\mathrm{d}\Phi_n}{\mathrm{d}z}+k_n\frac{\mathrm{d}^2\Phi_n}{\mathrm{d}z^2}\frac{\mathrm{d}\Phi_m}{\mathrm{d}z}\right]\right).
\end{aligned}\right\}\tag{2.16}$$

The forcing function R results from an interaction between various modes present at leading order, i.e. in the solutions for ψ_1, ρ_1 and v_1. The solution ψ_2 of the linear equation (2.15) is written in the same form as the two terms in the forcing function R:

$$\begin{aligned}
\psi_2 = &\sum_{m=-\infty}^{\infty}\sum_{n=-\infty}^{\infty}[h_{mn}(z)\cos((k_m+k_n)x-2\omega t\\
&+\alpha_m+\alpha_n)+g_{mn}(z)\cos((k_m-k_n)x+\alpha_m-\alpha_n)],
\end{aligned}\tag{2.17}$$

thus comprising superharmonic waves of frequency 2ω (and horizontal wavenumber k_m+k_n) and time-independent standing waves (and hence a non-zero mean flow) of horizontal wavenumber k_m-k_n. Substituting the solution form (2.17) into (2.15) generates the governing equation for $h_{mn}(z)$ and $g_{mn}(z)$. For a given modal pair (m,n), we define $\bar{h}_{mn}(z)=h_{mn}(z)+h_{nm}(z)$ and $\bar{g}_{mn}(z)=g_{mn}(z)+g_{nm}(z)$, which describe the vertical structure of the resulting superharmonic and time-independent terms, respectively, in ψ_2. The governing equations for $\bar{h}_{mn}(z)$ and $\bar{g}_{mn}(z)$ are

$$\frac{\mathrm{d}^2\bar{h}_{mn}}{\mathrm{d}z^2}+(k_m+k_n)^2\frac{N^2-4\omega^2}{4\omega^2-f^2}\bar{h}_{mn}=\bar{C}_{mn},\tag{2.18}$$

$$\frac{\mathrm{d}^2\bar{g}_{mn}}{\mathrm{d}z^2}-(k_m-k_n)^2\frac{N^2}{f^2}\bar{g}_{mn}=\bar{F}_{mn},\tag{2.19}$$

with the forcing functions being given by $\bar{C}_{mn}=-(A_{mn}+A_{nm})/(4\omega^2-f^2)$ and $\bar{F}_{mn}=(B_{mn}+B_{nm})/f^2$; $\bar{h}_{mn}(z)$ and $\bar{g}_{mn}(z)$ satisfy the boundary conditions $\bar{h}_{mn}(z=0)=\bar{h}_{mn}(z=$

$H) = \bar{g}_{mn}(z=0) = \bar{g}_{mn}(z=H) = 0$. A brief discussion on the mean flow vertical structure $\bar{g}_{mn}(z)$ is given in appendix A. In this paper, we focus our attention on $\bar{h}_{mn}(z)$, the vertical structure of the superharmonic nonlinear term.

For a given non-uniform stratification $N(z)$, $\bar{h}_{mn}(z)$ is calculated numerically by solving equation (2.18) along with the boundary conditions as a boundary value problem using the in-built Matlab function *bvp4c*. For a fixed stratification profile and (m, n), we compute $\bar{h}_{mn}^{max} = \max(|\bar{h}_{mn}(z)|)$ on a grid of 400×200 uniformly spaced points on the plane of $(\omega/N_0, f/\omega) \in [0.01, 0.99] \times [0.01, 0.99]$. For a given modal pair (m, n), we identify all the curves (referred to as the maxima curves) on the $(\omega/N_0, f/\omega)$ plane along which $\bar{h}_{mn}^{max}$ is a local maximum in a direction that is locally orthogonal to the curve. As discussed in § 3.2, we further verify that $\bar{h}_{mn}^{max}$ diverges in a very small neighbourhood around the maxima curves, which are henceforth termed divergence curves in the rest of this paper. Along every divergence curve we identify, the mode number s associated with the corresponding higher harmonic wave is calculated as $s = n_z + 1$, where n_z is the number of zeros for $\bar{h}_{mn}(z)$ in $z \in (0, H)$.

3. Results

We present results for an ocean-like non-uniform stratification profile $N(z)$ (figure 1*a*):

$$N(z) = N_0 + (N_{max} - N_0) \exp\left(-\frac{(z - z_c)^2}{\sigma^2}\right), \quad 0 \leqslant z \leqslant H, \tag{3.1}$$

where N_0 is the deep ocean uniform stratification and z_c is the centre of the pycnocline whose characteristic width and maximum stratification are σ and N_{max}, respectively; $z_c = 3400$ m and $\sigma = 250$ m are fixed throughout this paper, whereas N_{max} is varied to study the effects of pycnocline strength in § 3.2. For the specific case of $N_0 = 6 \times 10^{-4}$ rad s^{-1}, $N_{max} = 10N_0$, $\omega = 1.4053 \times 10^{-4}$ rad s^{-1} and $f = 0$, the vertical mode shapes $\Phi_n(z)$ (calculated by solving (2.12) numerically) for $n = 1, 2, 3$ are shown in figure 1(*b*); Φ_7 is plotted in figure 1(*c*). All the modes assume a sinusoidal form in the uniformly stratified deep ocean, and contain smaller vertical length scales in the pycnocline region.

3.1. *Uniform stratification* $(m \neq n)$

For a uniform stratification, i.e. $N(z) = N_{max} = N_0$ where N_0 is constant, equation (2.12) is solved analytically with the boundary conditions $\Phi_n(z = 0) = \Phi_n(z = H) = 0$ to obtain $\Phi_n(z) = \sin(n\pi z/H)$ and $k_n = n\pi/(H \cot\theta)$, where $\cot\theta = \sqrt{(N_0^2 - \omega^2)/(\omega^2 - f^2)}$. Substituting for $\Phi_n(z)$ and k_n, the particular solutions of (2.18) and (2.19) are

$$\bar{h}_{mn} = \bar{I}_{mn} \sin\left(\frac{(m-n)\pi z}{H}\right), \quad \bar{g}_{mn} = \bar{J}_{mn} \sin\left(\frac{(m+n)\pi z}{H}\right), \tag{3.2a,b}$$

where

$$\bar{I}_{mn} = \frac{4\pi\omega\sqrt{mnE_mE_n}}{\rho^* H^2(\omega^2 - f^2)} \left(\frac{(m^2 - n^2)\left(\frac{N_0^2}{2\omega\cot^2\theta} + \frac{\omega(N_0^2 - f^2)}{(\omega^2 - f^2)\cot^2\theta} + \frac{f^2}{2\omega}\right)}{(m+n)^2(N_0^2 - 4\omega^2) - (m-n)^2(4\omega^2 - f^2)\cot^2\theta}\right), \tag{3.3}$$

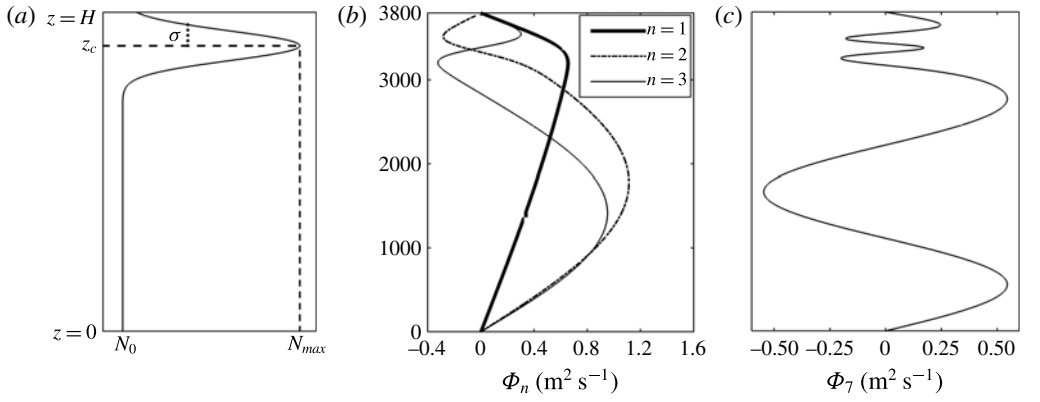

FIGURE 1. (*a*) The ocean-like stratification profile we consider in § 3. For the specific case of $N_0 = 6 \times 10^{-4}$ rad s^{-1}, $N_{max} = 10N_0$, $\omega = 1.4053 \times 10^{-4}$ rad s^{-1} and $f = 0$, the vertical mode shapes $\Phi_n(z)$ for (*b*) $n = 1, 2, 3$ and (*c*) $n = 7$ are shown. All the modes in (*b*) and (*c*) correspond to $E_n = 1$ W m^{-1}.

$$\bar{J}_{mn} = \frac{2\pi\sqrt{mnE_mE_n}}{\rho^* H^2(\omega^2 - f^2)\cot^2\theta}. \tag{3.4}$$

For a given (m, n), the coefficient $\bar{I}_{mn}$ in (3.2), and hence the superharmonic part of the weakly nonlinear solution, diverges if the condition $(m+n)^2(N_0^2 - 4\omega^2) - (m-n)^2(4\omega^2 - f^2)\cot^2\theta = 0$ is satisfied. Therefore, for fixed values of m, n and f/ω, the weakly nonlinear steady-state solution diverges for values of ω/N_0 given by

$$\frac{\omega^2}{N_0^2} = \frac{(m+n)^2 - (m-n)^2(4 - f^2/\omega^2)/(1 - f^2/\omega^2)}{4(m+n)^2 - (m-n)^2(4 - f^2/\omega^2)/(1 - f^2/\omega^2)}, \tag{3.5}$$

implying that no small-amplitude internal waves with non-zero strength in modes m and n at the frequency given by (3.5) can persist in their linear form. In the limit of $f = 0$, expression (3.5) is the same as what has been derived by Thorpe (1966). The expression in (3.5) can be equivalently derived by requiring the vertical mode number $|m - n|$ at frequency 2ω to correspond to a horizontal wavenumber of $k_m + k_n$, i.e. the two primary modes and the superharmonic wave form an internal wave resonant triad. It is noteworthy that there exists no such closed-form expressions or any other criterion for verification of resonance in non-uniform stratifications.

For at least one value of f/ω to exist in the range $0 \leqslant f/\omega < 1$ such that the corresponding ω/N_0 given by the expression in (3.5) satisfies $0 < \omega/N_0 < 1$, one requires the condition $(m+n)^2 > 4(m-n)^2$ to be satisfied. In other words, assuming a fixed frequency ω in the leading-order internal wave solution, divergence of the weakly nonlinear steady-state solution occurs for some $(\omega/N_0, f/\omega)$ (in the wave propagation regime) based on the interaction between modes m and n that satisfy

$$(m/3) < n < 3m, \quad m \neq n. \tag{3.6}$$

In figure 2, we plot the variation of $\log_{10}[\bar{h}_{mn}^{max}]$ as a function of ω/N_0 and f/ω for fixed values of $(E_m, E_n) = (0.9, 0.1)$ W m^{-1}, where $\bar{h}_{mn}^{max} = \max(|\bar{h}_{mn}(z)|)$. Figure 2(*a–c*) correspond to $(m, n) = (1, 2)$, $(2, 3)$ and $(2, 5)$, respectively, for the

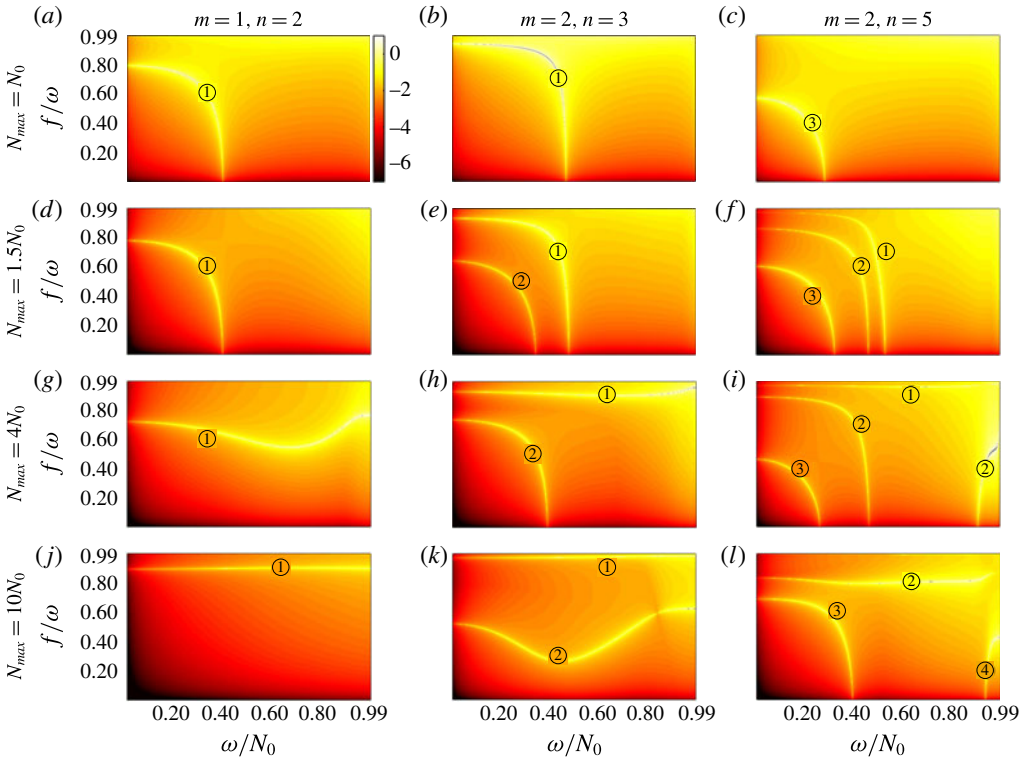

FIGURE 2. (Colour online) $\log_{10}[\bar{h}^{max}_{mn}]$ plotted as a function of ω/N_0 and f/ω for $(m, n) = (1, 2)$ (column 1), $(2, 3)$ (column 2) and $(2, 5)$ (column 3). The first, second, third and fourth rows correspond to $N_{max} = N_0$ (uniform stratification), $1.5N_0$, $4N_0$ and $10N_0$, respectively, in the stratification profile given by (3.1). The energy fluxes for each plot are fixed at $(E_m, E_n) = (0.9, 0.1)$ W m^{-1}. The mode numbers associated with the higher harmonic wave along the divergence curves are indicated by the encircled numbers. Note that the common colour bar (shown next to (a)) is saturated at a value of 1, hence making some of the divergence curves appear white.

uniform stratification ($N_{max} = N_0$). As shown in figure 2(a), there is a difference of a few orders of magnitude between regions close to and far from the divergence curve, which is described by (3.5). The divergence occurs at $\omega/N_0 = 0.395$ for $f/\omega = 0$ and then moves towards smaller values of ω/N_0 as f/ω is increased from zero. At approximately $f/\omega \approx 0.79$, the curve is almost horizontal, implying that strong nonlinear effects would occur over a wide range of ω/N_0 if modes 1 and 2 are simultaneously present. The peak occurring at the divergence curve is quite sharp if either ω/N_0 or f/ω is close to zero. In contrast, noticeably larger regions around the divergence curve correspond to large $\bar{h}^{max}_{mn}$ for values of ω/N_0 and f/ω away from zero, thus making the occurrence of strong nonlinear effects more likely. As evident in the solution for $\bar{h}_{mn}(z)$ in (3.2), the mode number of the higher harmonic wave on the divergence curves in a uniform stratification is always $|m - n|$.

For $(m, n) = (2, 3)$, shown in figure 2(b), the divergence curve occurs for larger values of ω/N_0 and f/ω compared to the case of $(m, n) = (1, 2)$. Interestingly, for $f/\omega \approx 0.935$, a wide range of values for ω/N_0 corresponds to infinitely large $\bar{h}_{23}(z)$; similarly, for $\omega/N_0 \approx 0.468$, a wide range of f/ω corresponds to large magnitudes of

$\bar{h}_{23}(z)$. The case of $(m, n) = (2, 5)$, shown in figure 2(*c*), is similar to that of $(m, n) = (1, 2)$ but with the divergence curve occurring at smaller values of ω/N_0 and f/ω. It is noteworthy that, for the uniform stratification, the divergence curve for $(m, n) = (2, 4)$ coincides with that of $(m, n) = (1, 2)$; also, based on condition (3.6), there exist no divergence curves for $(1, n \geqslant 3)$ and $(2, n \geqslant 6)$. Considering all possible modal interactions, described in detail in appendix C, all the divergence curves together span a significant portion of the plane $0 < \omega/N_0 < 0.5$, $0 < f/\omega < 1$. This suggests that modal interactions are highly likely to result in strong nonlinear effects irrespective of the specific values of ω/N_0 and f/ω. For $\omega/N_0 > 0.5$ in a uniform stratification, the higher harmonic wave at frequency 2ω can never represent a propagating internal wave, owing to which no resonant triads (and hence no divergence curves) exist for $\omega/N_0 > 0.5$. In contrast, in a non-uniform stratification with $N_{max} > N_0$, the higher harmonic wave at frequency 2ω can still represent a propagating internal wave as $2\omega/N < 1$ somewhere in the pycnocline. Thus, one cannot rule out the possibility of existence of divergence curves for $\omega/N_0 > 0.5$ if $N_{max} > N_0$.

3.2. *Non-uniform stratification* $(m \neq n)$

In figure 2(*d–l*), we show the variation of $\log_{10}[\bar{h}^{max}_{mn}]$ as a function of ω/N_0 and f/ω for fixed values of $(E_m, E_n) = (0.9, 0.1)$ W m^{-1} and three different non-uniform stratifications ($N_{max}/N_0 = 1.5$, 4 and 10 in the second, third and fourth rows of figure 2, respectively). We consider the same modal pairs as for the uniform stratification plots in figure 2(*a–c*). For $(m, n) = (1, 2)$, while the distribution of $\log_{10}[\bar{h}^{max}_{mn}]$ for the weak-pycnocline case of $N_{max} = 1.5N_0$ (figure 2*d*) is similar to that of $N_{max} = N_0$, the divergence curve deforms significantly for the intermediate pycnocline strength of $N_{max} = 4N_0$ (figure 2*g*) and also extends into the $\omega/N_0 > 0.5$ region. The divergence curve then becomes near horizontal for the strong-pycnocline case of $N_{max} = 10N_0$ (figure 2*j*), again spanning the entire range of $0 < \omega/N_0 < 1$. For $N_{max} = 10N_0$, strong nonlinear effects are therefore expected for all values of ω/N_0 at $f/\omega \approx 0.89$ as a result of the low-mode $(1, 2)$ interaction. As indicated by the encircled numbers on the divergence curves in figure 2(*a*,*d*,*g*,*j*), we find $\bar{h}_{mn}(z)$ to correspond to a mode-1 structure (based on the number of zeros in $z \in (0, H)$) along these curves for $(1, 2)$ interaction irrespective of N_{max}. Also noteworthy from figure 2(*a*,*d*,*g*,*j*) is the observation that small f/ω tends to correspond to no resonant triads for large N_{max}.

For $(m, n) = (2, 3)$, the number of divergence curves increases to two when N_{max} is increased from N_0 to $1.5N_0$ (figure 2*e*). The divergence curve along which $\bar{h}_{mn}(z)$ contains a mode-1 structure becomes near horizontal for $N_{max} = 4N_0$ (figure 2*h*), and is then horizontal and centred around $f/\omega = 0.97$ for $N_{max} = 10N_0$ (figure 2*k*). The second divergence curve corresponding to a mode-2 structure for the higher harmonic wave tends to become near horizontal at smaller values of f/ω as N_{max} is increased to $10N_0$. In summary, as N_{max} is increased from $1.5N_0$ to $10N_0$, both the divergence curves tend to become near horizontal at larger values of f/ω, and hence leave the regions of small f/ω with no divergence curves. For the higher-modes interaction, i.e. $(m, n) = (2, 5)$ shown in figure 2(*c*,*f*,*i*,*l*), we observe the existence of a larger number of divergence curves. For $N_{max} = 1.5N_0$, there are three different divergence curves (with three different modal structures for $\bar{h}_{mn}$), which is in stark contrast to the existence of only one divergence curve for $N_{max} = N_0$. An additional mode-2 divergence curve emerges in the region of large ω/N_0 for $N_{max} = 4N_0$. Similarly, a mode-4 divergence curve occurs at large ω/N_0 for $N_{max} = 10N_0$. It is noteworthy that as N_{max} increases, the range of ω/N_0 where the higher harmonic wave at frequency

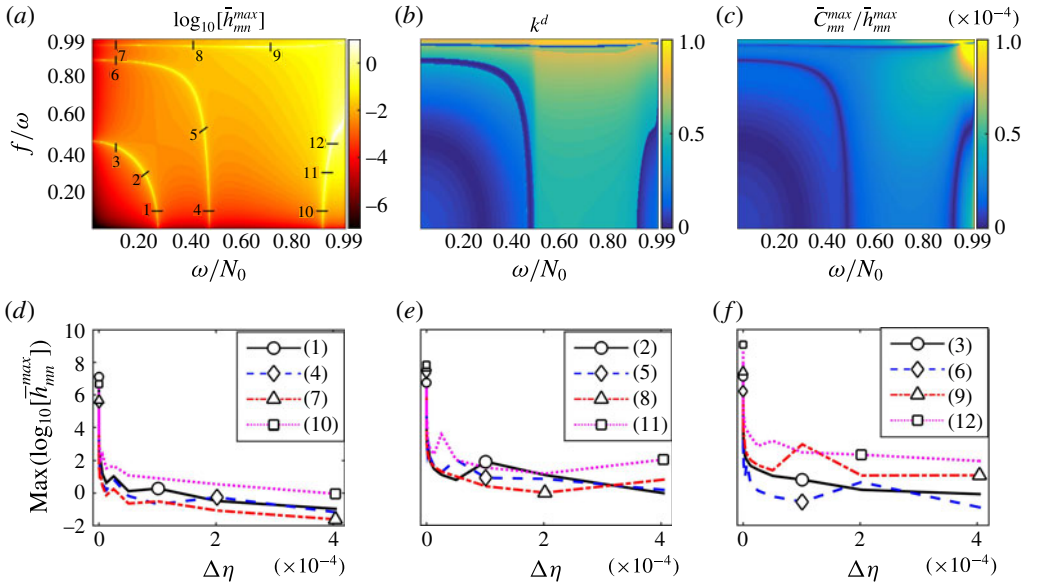

FIGURE 3. (Colour online) (*a*) $\log_{10}[\bar{h}^{max}_{mn}]$ plotted as a function of ω/N_0 and f/ω for $(m, n) = (2, 5)$, $N_{max} = 4N_0$ and $(E_m, E_n) = (0.9, 0.1)$ W m^{-1}, the same case as in figure 2(*i*). Corresponding distributions of (*b*) $k^d = |k_m + k_n - k_q^{2\omega}|/k_q^{2\omega}$ and (*c*) $\bar{C}^{max}_{mn}/\bar{h}^{max}_{mn}$ are also shown. The various cross-sectional cuts (across the divergence curves) that are considered in the bottom row of panels are shown using black solid lines and indexed from 1 to 12 in (*a*). (*d–f*) Detected maximum value of $\log_{10}[\bar{h}^{max}_{mn}]$ as a function of the grid size $\Delta\eta$ (η is the coordinate measured along the cut) on the 12 cross-sectional cuts shown in (*a*). The legend in each of (*d–f*) indicates the cross-section index associated with each curve. Each curve in (*d–f*) contains 25 points in the range $2.38 \times 10^{-11} \leqslant \Delta\eta \leqslant 4 \times 10^{-4}$.

2ω can represent a propagating internal wave increases, thus allowing for additional divergence curves to emerge at large ω/N_0. An overall summary from figure 2 is that, for a given modal pair (m, n), regions of small and large f/ω tend to correspond to smaller and larger numbers of resonant triads, respectively.

To verify that pure resonant triads indeed exist along the various divergence curves of $\bar{h}_{mn}(z)$, we analyse the case of $(m, n) = (2, 5)$ and $N_{max} = 4N_0$ more closely in figure 3. Plotted in figure 3(*a*) is $\log_{10}[\bar{h}^{max}_{mn}]$ as a function of ω/N_0 and f/ω, showing divergence along four different curves. In figure 3(*b*), we plot k^d, the relative difference between $k_m + k_n$ and the numerically computed horizontal wavenumber $k_q^{2\omega}$ of mode-q at frequency 2ω, where $q - 1$ is the number of zeros of $\bar{h}_{mn}(z)$ in $z \in (0, H)$. Indeed, k^d attains very small values along the four curves where $\bar{h}_{mn}(z)$ is divergent, suggesting that the horizontal wavenumber $k_m + k_n$ of the superharmonic wave matches that of mode-q at frequency 2ω along the divergence curves. To confirm if the superharmonic wave is indeed an internal wave mode along the divergence curves, one also has to compare the vertical structure of $\bar{h}_{mn}(z)$ with that of internal wave mode-q at frequency 2ω. We recall that $\bar{h}_{mn}(z)$ is governed by (2.18), whose left-hand side coincides with that of the governing equation for internal

wave mode-q ($\Phi_q^{2\omega}$) at frequency 2ω if $k_m + k_n = k_q^{2\omega}$:

$$\frac{\mathrm{d}^2\Phi_q^{2\omega}}{\mathrm{d}z^2} + \frac{(k_q^{2\omega})^2(N^2 - (2\omega)^2)}{(2\omega)^2 - f^2}\Phi_q^{2\omega} = 0. \tag{3.7}$$

The right-hand side of (2.18) is, however, non-zero, and specified by $\bar{C}_{mn}(z)$. In figure 3(*c*), we plot $\bar{C}_{mn}^{max}/\bar{h}_{mn}^{max}$, which is a measure of the extent to which the normalized vertical structure of the superharmonic wave, $\bar{h}_{mn}(z)/\bar{h}_{mn}^{max}$, satisfies (3.7) if $k_q^{2\omega} = k_m + k_n$. Figure 3(*c*) shows that $\bar{C}_{mn}^{max}/\bar{h}_{mn}^{max}$ is very small along the divergence curves, and together with figure 3(*b*) confirms that the superharmonic wave is an internal wave along the divergence curves observed in figure 3(*a*). Furthermore, it seems that the condition $k^d \ll 1$ alone is a sufficiently accurate measure of how close a given $(\omega/N_0, f/\omega)$ is to a divergence curve. The calculation of k^d still requires the value of q, which can only come from the numerical solution of (2.18) to obtain $\bar{h}_{mn}(z)$. A detailed discussion of the relation between figure 3(*a–c*) and the existence of pure resonant triads is presented in § 3.4.

To verify that $\bar{h}_{mn}(z)$ indeed diverges on the divergence curves, we calculate $\bar{h}_{mn}^{max}$ on very small domains in the neighbourhood of the divergence curves seen in figure 3(*a*). As shown in figure 3(*a*), we consider cross-sectional cuts (1–12) across the various divergence curves, with η defining the coordinate along these cuts. In figure 3(*d–f*), we plot the detected maximum value (within the corresponding cut) of $\log_{10}\bar{h}_{mn}^{max}$ as a function of the resolution $\Delta\eta$ along the 12 different cuts. Each curve in figure 3(*d–f*) contains 25 points in the range $2.38 \times 10^{-11} \leqslant \Delta\eta \leqslant 4 \times 10^{-4}$. The legend in each of figure 3(*d–f*) indicates the specific cut (indexed in figure 3*a*) that each curve is associated with. For every curve in figure 3(*d–f*), we observe an increase in $\max[\bar{h}_{mn}^{max}]$ by six orders of magnitude when $\Delta\eta$ is decreased from 4×10^{-4} to 2.38×10^{-11}. This suggests strongly that the numerically identified divergence curves in figure 3(*a*) do correspond to divergence in $\bar{h}_{mn}(z)$ in their close vicinity. We have further verified that a similar result holds for all the divergence curves shown in figure 2.

3.3. *Self-interaction* ($m = n$)

For self-interactions, i.e. $m = n$, the right-hand side $\bar{C}_{mm}$ in (2.18) reduces to $-2E_m k_m^4 \phi_m^2 (\mathrm{d}N^2/\mathrm{d}z)/[\rho^*(\omega^2 - f^2)^2 \int_0^H (\mathrm{d}\Phi_m/\mathrm{d}z)^2\,\mathrm{d}z]$, thus resulting in a non-zero right-hand side in (2.18) for non-uniform stratifications only. An equivalent expression for self-interaction was also derived by Diamessis *et al.* (2014) and Wunsch (2015), with the latter study considering an individual mode at frequency ω as the primary wave, albeit with no background rotation. Wunsch (2015) then calculated the amplitude of the higher harmonic wave at frequency 2ω for an idealized non-uniform stratification with a sharp interface modelling the pycnocline, to subsequently compare with the field observations of Xie *et al.* (2013). The generation of superharmonics as a result of self-interaction in a mode-1 internal wave in non-uniform stratifications was also reported in a recent numerical study by Sutherland (2016).

In figure 4(*a–c*), we plot $\log_{10}[\bar{h}_{mm}^{max}]$ as a function of ω/N_0 and f/ω for $m = 1, 3, 5$ in a non-uniform stratification with $N_{max} = 4N_0$. Self-interaction of mode-1 shows no divergence curve in figure 4(*a*), with $\bar{h}_{mm}^{max}$ increasing as a function of both ω/N_0 and f/ω. For $m = 3$, however, there exist three different divergence curves, as shown in figure 4(*b*). Two of these divergence curves correspond to a mode-2 superharmonic wave, whereas the one that is near horizontal at $f/\omega \approx 0.9$ corresponds to a mode-1

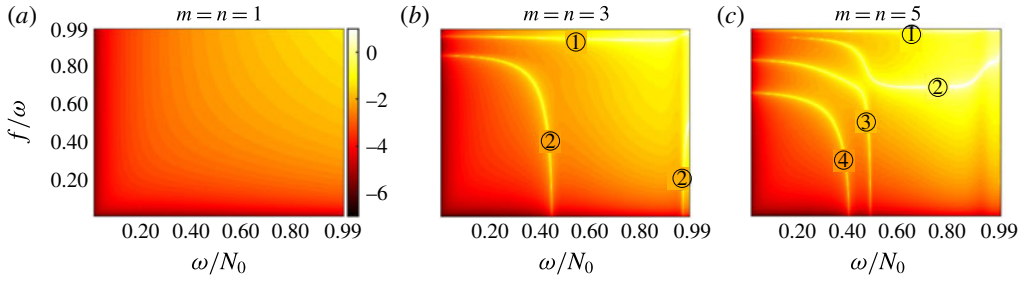

FIGURE 4. (Colour online) $\log_{10}[\bar{h}^{max}_{mn}]$ plotted as a function of ω/N_0 and f/ω for (*a*) $(m, n) = (1, 1)$, (*b*) $(m, n) = (3, 3)$ and (*c*) $(m, n) = (5, 5)$. All panels correspond to the stratification profile given in (3.1) with $N_{max} = 4N_0$ and $(E_m, E_n) = (0.9, 0.1)$ W m^{-1}. The mode numbers associated with the higher harmonic wave along the divergence curves are indicated by the encircled numbers.

superharmonic wave. Self-interaction of mode-5 is even more complex, and results in four different divergence curves with distinct mode numbers for the superharmonic wave (figure 4*c*). In summary, figure 4(*b–c*) show that even individual modes can be unstable linear internal wave forms irrespective of their amplitude if ω/N_0 and f/ω lie on any of the divergence curves.

3.4. *Criteria for triadic resonance*

Here, we discuss the general conditions under which divergence of $\bar{h}_{mn}(z)$ occurs on the $(\omega/N_0, f/\omega)$ plane. The governing equation (2.18) for $\bar{h}_{mn}(z)$ is rewritten as

$$\frac{\mathrm{d}^2\bar{h}_{mn}}{\mathrm{d}z^2} + r^2 L^{2\omega}(z)\bar{h}_{mn} = \bar{C}_{mn}, \tag{3.8}$$

where $r = k_m + k_n$, $L^{2\omega}(z) = (N^2 - 4\omega^2)/(4\omega^2 - f^2)$ and $\bar{C}_{mn}$ is as described in the text following (2.18). The general solution for (3.8) is written as $\bar{h}_{mn}(z) = \bar{h}^h_{mn}(z) + \bar{h}^p_{mn}(z)$, where $\bar{h}^h_{mn}(z)$ and $\bar{h}^p_{mn}(z)$ are the homogeneous and particular solutions, respectively.

The homogeneous solution $\bar{h}^h_{mn}(z)$ satisfies the equation

$$\frac{\mathrm{d}^2\bar{h}^h_{mn}}{\mathrm{d}z^2} + r^2 L^{2\omega}(z)\bar{h}^h_{mn} = 0. \tag{3.9}$$

A non-zero homogeneous solution $\bar{h}^h_{mn}(z)$ exists if and only if $r = k_m + k_n$ equals the horizontal wavenumber $k_s^{2\omega}$ associated with an internal wave mode (say mode-s) at frequency 2ω. The vertical modes at frequency 2ω are denoted by $Q_j^{2\omega}(z)$ with j being the mode number and $k_j^{2\omega}$ the corresponding horizontal wavenumber.

The particular solution $\bar{h}^p_{mn}(z)$ satisfies (3.8). Using $Q_j^{2\omega}(z)$, $1 \leqslant j \leqslant \infty$, as a complete set of basis functions, we write the particular solution as

$$\bar{h}^p_{mn}(z) = \sum_{j=1}^{\infty} \alpha_j Q_j^{2\omega}(z), \tag{3.10}$$

where the basis functions $Q_j^{2\omega}(z)$ satisfy the orthogonality condition

$$\int_0^H L^{2\omega}(z)Q_i^{2\omega}(z)Q_j^{2\omega}(z)\,\mathrm{d}z = 0, \quad i \neq j \tag{3.11}$$

and $\alpha_j \in (-\infty, \infty)$ represents the amplitude of $Q_j^{2\omega}(z)$. Substituting (3.10) into the governing equation (3.8), we obtain

$$\sum_{j=1}^{\infty} \alpha_j (r^2 - (k_j^{2\omega})^2) L^{2\omega}(z) Q_j^{2\omega}(z) = \bar{C}_{mn}(z). \tag{3.12}$$

We note that (3.12) has incorporated the governing equation for $Q_j^{2\omega}(z)$, i.e. $\mathrm{d}^2 Q_j^{2\omega}/\mathrm{d}z^2 + (k_j^{2\omega})^2 L^{2\omega} Q_j^{2\omega} = 0$.

Using the orthogonality condition in (3.11), equation (3.12) reduces to

$$\alpha_j (r^2 - (k_j^{2\omega})^2) = \frac{\displaystyle\int_0^H \bar{C}_{mn}(z) Q_j^{2\omega}(z)\,\mathrm{d}z}{\displaystyle\int_0^H L^{2\omega}(z)(Q_j^{2\omega}(z))^2\,\mathrm{d}z} \tag{3.13}$$

for all j. If a non-zero homogeneous solution $\bar{h}_{mn}^h(z)$ exists, i.e. $r = k_j^{2\omega}$ for some $j = s$, then (3.13) requires that $\int_0^H \bar{C}_{mn}(z) Q_s^{2\omega}(z)\,\mathrm{d}z = 0$, i.e. $\bar{C}_{mn}(z)$ being orthogonal to $Q_s^{2\omega}(z)$ must be satisfied. In other words, a non-zero $\bar{h}_{mn}^h(z)$ together with the non-orthogonality condition $\int_0^H \bar{C}_{mn}(z) Q_s^{2\omega}(z)\,\mathrm{d}z \neq 0$ imply that $\alpha_s \to \infty$, thus resulting in a diverging solution of (3.8). In summary, $r = k_m + k_n$ being the horizontal wavenumber of some mode-s at frequency 2ω is necessary but not sufficient for triadic resonance; the additional criterion of non-orthogonality of the right-hand side of (3.8) to the homogeneous solution $Q_s^{2\omega}(z)$ is also required. This additional criterion of non-orthogonality, in the limit of a uniform stratification, is equivalent to the vertical wavenumbers satisfying the classic triadic resonance criterion $\boldsymbol{k}_1 + \boldsymbol{k}_2 + \boldsymbol{k}_3 = 0$.

In a non-uniform stratification, the identification of regions/curves on the $(\omega/N_0, f/\omega)$ plane where a non-zero homogeneous solution exists for a given modal interaction is computationally involved. This is mainly owing to the fact that the value of s, the mode number associated with the homogeneous solution that may exist, is unknown *a priori*. For example, an interaction between mode-2 and mode-5 can result in a higher harmonic wave whose mode number is any value between 1 and 4 (figure 2*f,i,l*) if the stratification is non-uniform. In contrast, for uniform stratifications, the mode number associated with the higher harmonic wave is always $|m-n|$ on the divergence curves. Furthermore, the verification of the non-orthogonality between $\bar{C}_{mn}(z)$ and $Q_s^{2\omega}(z)$ involves setting an arbitrary threshold on the value of $\int_0^H \bar{C}_{mn}(z) Q_s^{2\omega}(z)\,\mathrm{d}z$ below which the functions can be deemed orthogonal. In our approach presented in §§ 3.1–3.3, we directly compute the particular solution $\bar{h}_{mn}^p(z)$ and plot its magnitude on the entire $(\omega/N_0, f/\omega)$ plane, thus allowing us to easily identify the divergence curves along which triadic resonance occurs without the requirement of *a priori* knowledge of s or any arbitrary thresholds. The mode number s associated with the higher harmonic wave that forms a resonant triad with modes m and n at frequency ω is obtained from the numerically computed vertical structure of $\bar{h}_{mn}^p(z)$ at the locations of the divergence curves on the $(\omega/N_0, f/\omega)$ plane.

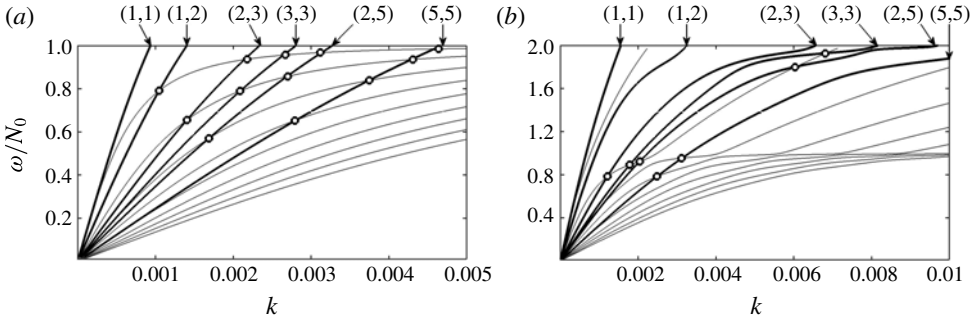

FIGURE 5. Dispersion curves (thin grey solid lines) ω/N_0 as a function of k for modes 1–9 (from left to right) for (*a*) $N_{max} = N_0$ (uniform stratification) and (*b*) $N_{max} = 4N_0$. The thick black solid lines in both (*a*) and (*b*) show the variation of $2\omega/N_0$ with $k_m + k_n$ for the (m, n) combination indicated at the top for each curve. The points of intersection between the black curves and the grey curves are shown using the ∘ marker. Both panels correspond to $f/\omega = 0.2$.

We now proceed to demonstrate, for fixed N_{max}/N_0 and f/ω, the identification of values of ω/N_0 at which a non-zero homogeneous solution $\bar{h}^h_{mn}(z)$ exists. In figure 5(*a*), we plot in grey the dispersion curves, i.e. ω/N_0 versus k, corresponding to modes 1–9 for a uniform stratification ($N_{max} = N_0$) and $f/\omega = 0.2$. These dispersion curves, with mode-1 being the leftmost and mode-9 the rightmost curve, are known analytically for the uniform stratification (see § 3.1). Plotted as black solid curves in figure 5(*a*) are the variations of $2\omega/N_0$ with $k_m + k_n$ for the values of (m, n) indicated on top of each of the curves. Points of intersection between the black curves and the grey curves occur at values of ω/N_0 for which a non-zero homogeneous solution exists, i.e. $k_m + k_n$ equals the horizontal wavenumber of some mode-s at frequency 2ω; s is the mode number associated with the grey line passing through the corresponding point of intersection.

In figure 5(*a*), the black curve corresponding to $(m, n) = (1,1)$ intersects with none of the grey dispersion curves, and hence no resonant interaction occurs for the self-interaction of mode-1. Self-interaction of mode-3, i.e. the black curve associated with $(3, 3)$, intersects the mode-1 and mode-2 dispersion curves. No divergence of the weakly nonlinear solution occurs at these two points of intersection as $\bar{C}_{33}(z)$ is uniformly zero for a uniform stratification (see § 3.3), i.e. the additional non-orthogonality criterion of $\int_0^H \bar{C}_{33}(z) Q_s^{2\omega}(z)\,\mathrm{d}z \neq 0$ is not satisfied for both $s = 1$ and $s = 2$. A similar conclusion holds for the self-interaction of mode-5, where there is no divergence of $\bar{h}_{55}(z)$ at all four points of intersection with the dispersion curves. Analytical expressions identifying values of $(\omega/N_0, f/\omega)$ at which non-zero $\bar{h}^h_{mm}(z)$ exists for self-interaction in a uniform stratification are given in appendix B. In summary, self-interaction in a uniform stratification can result in higher harmonic internal wave generation along specific curves on the $(\omega/N_0, f/\omega)$ plane, but can never result in triadic resonance as $\bar{C}_{mm}(z)$ is uniformly zero.

For $m \neq n$ in a uniform stratification, i.e. the cases $(m, n) = (1, 2)$, $(2, 3)$ and $(2, 5)$ in figure 5(*a*), the black curves always intersect with the dispersion curve associated with mode number $s = |m - n|$. The non-orthogonality criterion is further satisfied at these points of intersection, thus resulting in the divergence of $\bar{h}_{mn}(z)$ as shown in figure 2(*a–c*) (consider variation along the horizontal line $f/\omega = 0.2$ in figure 2*a–c*).

For $(m, n) = (2, 3)$ and $(2, 5)$ in figure 5(*a*), there are additional points of intersection of the black curves with the dispersion curves corresponding to modes different from $|m - n|$. At these additional points of intersection, no divergence (or even a local maximum) of $\bar{h}_{mn}(z)$ occurs (figure 2*a–c*) as the non-orthogonality criterion is not satisfied. In summary, for $m \neq n$ in a uniform stratification, the existence of non-zero $\bar{h}^h_{mn}(z)$, which guarantees the satisfaction of the horizontal component of the classic triadic resonance criterion $\boldsymbol{k}_1 + \boldsymbol{k}_2 + \boldsymbol{k}_3 = 0$, is not sufficient for triadic resonance to occur.

In figure 5(*b*), we perform the same analysis as in figure 5(*a*) for the non-uniform stratification with $N_{max} = 4N_0$. For self-interaction of mode-1, i.e. $(m, n) = (1, 1)$, the black curve does not intersect with any of the dispersion curves, consistent with the occurrence of no divergence curves in figure 4(*a*). For $(m, n) = (3, 3)$, two intersections occur with the mode-2 dispersion curve, with corresponding divergences of $\bar{h}_{33}(z)$ seen for two different values of ω/N_0 along $f/\omega = 0.2$ in figure 4(*b*). Similarly, for all the other modal interactions considered in figure 5(*b*), all the intersections with the dispersion curves correspond to the divergence of $\bar{h}_{mn}(z)$ in figures 2(*g–i*) and 4(*c*). Furthermore, there is agreement between figure 5(*b*) and figures 2(*g–i*) and 4 in terms of both the locations of intersections/divergence and the mode number associated with the higher harmonic wave at these locations. We have also verified numerically that the non-orthogonality criterion is satisfied at all the points of intersection in figure 5(*b*). In summary, for non-uniform stratifications, it seems that the existence of a non-zero homogeneous solution $\bar{h}^h_{mn}(z)$ alone guarantees the occurrence of triadic resonance at the corresponding locations on the $(\omega/N_0, f/\omega)$ plane. In other words, it seems unlikely that $C_{mn}(z)$ will be exactly orthogonal to the corresponding $Q_s^{2\omega}(z)$ in a non-uniform stratification, thus significantly increasing the number of triadic resonances on the $(\omega/N_0, f/\omega)$ plane in comparison to the uniform stratification for a given modal interaction. Furthermore, the existence of $\bar{h}^h_{mn}(z)$ being sufficient for triadic resonance suggests that an infinitely greater number of modal interactions in non-uniform stratifications result in divergence curves on the $(\omega/N_0, f/\omega)$ plane when compared to uniform stratifications.

Numerical calculation of $\bar{h}_{mn}(z)$ on the entire $(\omega/N_0, f/\omega)$ plane for a given modal interaction, as done in §§ 3.1–3.3, allows us to directly identify curves along which triadic resonance occurs. This is in contrast to the multiple steps involved in the approach presented in figure 5, which has to be repeated for all values of $f/\omega \in (0, 1)$ to obtain curves of triadic resonance on the entire $(\omega/N_0, f/\omega)$ plane. Also, computing the vertical structure of $\bar{h}_{mn}(z)$ gives the value of the mode number q of the higher harmonic internal wave mode that may be in triadic resonance with modes m and n at frequency ω. Therefore, in the case of a non-uniform stratification, for which the existence of non-zero $\bar{h}^h_{mn}(z)$ seems sufficient to identify triadic resonance, the problem reduces to a simple calculation of the relative difference between $k_m + k_n$ and $k_q^{2\omega}$. We adopt this approach of calculating $\bar{h}_{mn}(z)$, then estimating q, followed by a calculation of $k^d = |k_m + k_n - k_q^{2\omega}|/k_q^{2\omega}$ in § 4.2.

4. Discussion

The theoretical framework developed in this paper is potentially relevant for several oceanic scenarios. Here, we implement our theoretical calculations on idealized models of the linear wave fields that result from (i) low-mode internal tide scattering by topography (§ 4.1) and (ii) internal wave beams generated by tidal flow over topography (§ 4.2), both in non-uniform stratifications containing a pycnocline.

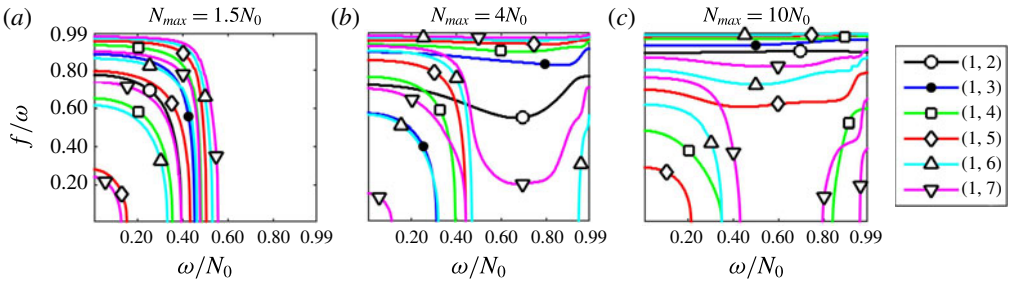

FIGURE 6. (Colour online) (*a*) Plots of divergence curves on the $(\omega/N_0, f/\omega)$ plane where $\bar{h}_{mn}(z)$ diverges for $(m, n) = (1, n)$ $(2 \leqslant n \leqslant 7)$ in a non-uniform stratification with (*a*) $N_{max} = 1.5N_0$, (*b*) $N_{max} = 4N_0$ and (*c*) $N_{max} = 10N_0$. Each n corresponds to a separate colour and marker style, as indicated in the legend on the right. Among the modal interactions considered in this figure, only $(m, n) = (1, 2)$ corresponds to the presence of a divergence curve for a uniform stratification.

4.1. *Mode-1 scattering by bottom topography*

In general, the high- and low-mode content of semidiurnal internal tides are understood, respectively, to dissipate close to and propagate far from their topographic generation sites. The mode-1 internal tides that tend to travel far from their generation sites encounter long stretches of small-scale (and sometimes large-scale) rough topography. The resulting interaction between mode-1 and the topography can scatter an appreciable amount of energy into higher modes at the semidiurnal frequency (Bühler & Holmes-Cerfon 2011; Mathur *et al.* 2014), raising questions about the nonlinear effects that may result from interaction between mode-1 and higher modes. For example, to the north of Hawaii, the mode-1 internal tide is estimated to lose approximately 10 % of its energy to higher modes upon propagation over 2000 km of small-scale topography (Mathur *et al.* 2014). In contrast, to the south of Hawaii, the mode-1 internal tide can lose up to 40 % of its energy to higher modes at the Line Islands Ridge (Johnston *et al.* 2003). We note here that the initiation of a modal interaction, especially close to triadic resonance, depends only on the presence of some non-zero energy in the primary waves.

As shown in § 3.1, divergence of $\bar{h}_{mn}(z)$ occurs only for $(m/3) < n < 3m$ in the case of a uniform stratification. Mode-1 can therefore resonantly interact only with mode-2 in a uniform stratification. This result, however, is not necessarily true for non-uniform stratifications. We therefore proceed to compute the divergence curves, if any, for mode-1 interactions with various higher modes ($\geqslant 2$). Specifically, in figure 6, we consider interactions resulting from modes $(m, n) = (1, n)$ $(2 \leqslant n \leqslant 7)$ in the non-uniform stratification described by (3.1). Figure 6(*a–c*) show the divergence curves for $N_{max} = 1.5N_0$, $4N_0$ and $10N_0$, respectively. Interestingly, $(m, n) = (1, 3)$ corresponds to the presence of a divergence curve even for the weak-pycnocline case of $N_{max} = 1.5N_0$. In figure 6(*a*), the divergence curves corresponding to the interaction of mode-1 with modes 2–7 span a significant portion of the domain $0 < \omega/N_0 \lessapprox 0.5$, $0 < f/\omega < 1$. It is therefore likely that strong nonlinear effects occur for any $(\omega/N_0 < 0.5, f/\omega)$ as long as there exist mechanisms by which at least a small amount of mode-1 energy is put into modes 2–7. Of significance is the presence of at least one divergence curve for all the modal interactions we consider in figure 6(*a*). Furthermore, multiple divergence curves occur for a fixed (m, n) where $m = 1$ and $4 \leqslant n \leqslant 7$. In fact, (1, 7) interaction

corresponds to four different divergence curves in figure 6(*a*). We recall that a given (m, n) interaction can result in at most one divergence curve on the $(\omega/N_0, f/\omega)$ plane for a uniform stratification.

For $N_{max} = 4N_0$ (figure 6*b*), there is again a large number of divergence curves, now spread over the entire $(\omega/N_0, f/\omega)$ plane, for $m = 1$ and $2 \leqslant n \leqslant 7$, with some of them being horizontal at large f/ω even for small n. For the strongest-pycnocline case of $N_{max} = 10N_0$ (figure 6*c*), low-mode interactions $(m, n) = (1, 2), (1, 3)$ result in near-horizontal divergence curves at $f/\omega = 0.89, 0.93$, respectively. The interaction of mode-1 with higher modes ($n = 4$–7) again leads to more divergence curves that span a wide range of ω/N_0 and f/ω. In summary, RTIs are likely to occur in the ocean as a result of interaction between mode-1 and the higher modes generated by topographic scattering of mode-1. An interesting observation from figure 6 is the contrasting effect of increasing N_{max} on the number of divergence curves in the small-f/ω region of the $(\omega/N_0, f/\omega)$ plane. For $\omega/N_0 < 0.5$, for which the higher harmonic wave at 2ω is propagating throughout the ocean depth, the number of divergence curves passing through the $f/\omega = 0$ line noticeably decreases with an increase in N_{max}. In contrast, for $\omega/N_0 > 0.5$, for which internal wave propagation at 2ω is restricted to the pycnocline region, the number of divergence curves passing through $f/\omega = 0$ increases with an increase in N_{max}. In summary, figure 6 suggests that a significantly larger number of resonant mode interactions occur in a non-uniform stratification compared to a uniform stratification.

It may be potentially interesting to include primary waves that propagate in the negative x-direction to model interaction between incident and reflected waves at topographic sites. The dissipation of high-mode internal tides close to the generation sites can also be initiated by a nonlinear transfer of energy to higher frequencies and smaller length scales that result from modal interactions at the semidiurnal frequency. Finally, the existence of RTI arising from modal interactions raises questions about the validity of linear models of generation and scattering that assume a range of vertical modes at a fixed frequency in the wave field.

4.2. *Internal wave beam incident on a pycnocline*

The generation of mean flow and superharmonics shown in this paper is strikingly similar to the nonlinear effects that result from colliding plane waves or wave beams, a prevalent occurrence when an internal wave beam interacts with either a solid boundary (Peacock & Tabaei 2005) or a free-slip surface (Zhou & Diamessis 2013) or with the ocean pycnocline (Grisouard, Staquet & Gerkema 2011; Mercier *et al.* 2012). It may therefore be worthwhile to model these occurrences as nonlinear interaction between modes rather than as localized interaction between colliding plane waves or wave beams. For example, the qualitative differences in harmonic wave generation observed for various pycnoclines (Diamessis *et al.* 2014) could be explained using a modal representation of the incident wave beam, which we now proceed to elucidate further.

As shown in figure 7, Diamessis *et al.* (2014) numerically studied the dynamics of an upward-propagating internal wave beam of dominant wavelength λ_x in the constant deep ocean stratification N_0 incident on a pycnocline whose thickness is h and where the maximum stratification is denoted by N_{max}. The stratification profile and the incident wave beam profile are both described in Diamessis *et al.* (2014). The incident wave frequency was specified as $\omega = N_0/\sqrt{2}$ corresponding to a 45° wave beam, which corresponds to the first higher harmonic 2ω being evanescent in

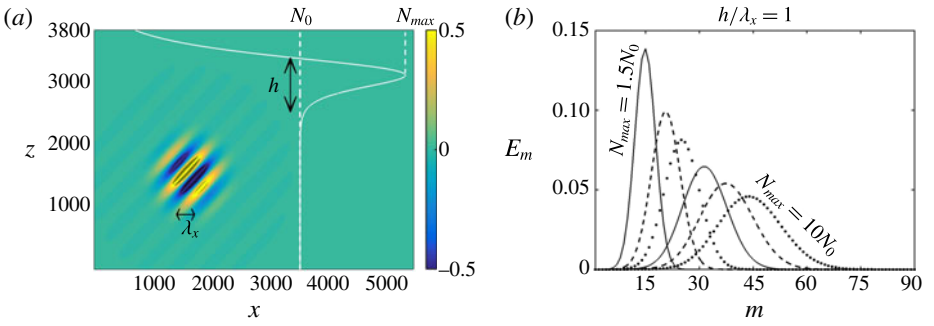

FIGURE 7. (Colour online) (*a*) Schematic depicting the flow studied by Diamessis *et al.* (2014) and discussed in § 4.2. An upward-propagating wave beam of dominant horizontal wavelength λ_x in a stratification N_0 is incident on a pycnocline of thickness h and maximum stratification N_{max}. (*b*) Energy flux fraction E_m in mode-m for various pycnocline strengths ($N_{max} = (1.5, 3, 4, 6, 8, 10)N_0$ from left to right) and a fixed pycnocline thickness given by $h/\lambda_x = 1$.

the deep ocean. It was shown that higher harmonics were invariably generated as a result of the interaction between the incident wave beam and the pycnocline, with the amplitude and number of higher harmonics increasing with N_{max}/N_0 for a given normalized pycnocline thickness h/λ_x.

For a thin pycnocline, i.e. $h/\lambda_x = 0.1$, it was shown by Diamessis *et al.* (2014) that the amplitudes of the higher harmonics were largest when their frequencies and wavenumbers satisfy the interfacial wave dispersion relation. They then proceed to construct a theoretical model that considers a plane internal wave incident on a sharp interface across which there is a density jump, with no boundaries either below or above the sharp interface. Interfacial waves are relevant only in the limit of extremely thin pycnoclines and with the primary wave frequency ω satisfying $2\omega > N_0$, thus rendering the higher harmonics evanescent in the deep ocean. In our theoretical framework, the influence of the boundaries both below and above the pycnocline is completely accounted for, and there are no assumptions about either the pycnocline thickness or the primary wave frequency. In the limit of $h/\lambda_x \ll 1$, $2\omega > N_0$ and the ocean boundaries being far from the pycnocline, the existence of a resonant triad with two modes at frequency ω and the third at frequency 2ω is equivalent to the requirement of the higher harmonics having to satisfy the interfacial wave dispersion relation. Furthermore, the presence of boundaries above and below the thin pycnocline restricts the number of interfacial mode wavenumbers to be countably infinite, as opposed to the possibility of a continuous range of wavenumbers when there are no boundaries. In summary, the thin-pycnocline results of Diamessis *et al.* (2014) reaffirm our conclusion that the existence of a resonant triad results in the amplification of the higher harmonics.

For a thick pycnocline, i.e. $h/\lambda_x = 1$, Diamessis *et al.* (2014) observe harmonic generation at multiple locations in the pycnocline, thus resulting in a complex flow pattern. Here, we present the results of our analysis for six different values of N_{max}/N_0 with a fixed normalized pycnocline thickness of $h/\lambda_x = 1$. In figure 7(*b*), we show the fractional distribution of energy fluxes in various modes corresponding to the incident wave beam in figure 7(*a*). The energy flux distribution moves rightwards to higher modes as N_{max}/N_0 is increased from 1.5 to 10. For each of the six N_{max}/N_0 values, we

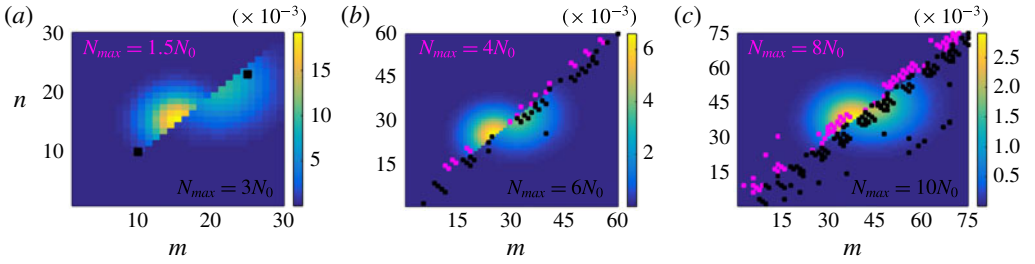

FIGURE 8. (Colour online) The product E_mE_n shown in colour as a function of m and n for the incident wave beam shown in figure 7 and for (*a*) $N_{max} = (1.5, 3)N_0$, (*b*) $N_{max} = (4, 6)N_0$ and (*c*) $N_{max} = (8, 10)N_0$. In each plot, the small and large N_{max} cases are shown at the top left and bottom right, respectively. The pink (top left) and black (bottom right) points mark the (m, n) combinations for which $k^d = |(k_m + k_n - k_q^{2\omega})|/k_q^{2\omega}$ is less than 0.01 for the corresponding stratification, indicating that the (m, n) pair of modes at frequency ω could form a resonant triad with mode-q at frequency 2ω.

explore the existence of resonant triads containing a pair of modes (m, n) (with non-negligible E_m and E_n) at the primary wave frequency ω. The existence of a resonant triad is established by verifying if the condition $k^d = |(k_m + k_n - k_q^{2\omega})|/k_q^{2\omega} = 0$ is satisfied within a specified limit. Here, q is calculated as $q = n_z + 1$, where n_z is the number of zeros in $h_{mn}(z)$. We recall from figure 3 and § 3.4 that regions of small values of k^d indeed capture the regions in the neighbourhood of divergence curves/triadic resonance.

In figure 8(*a–c*), we show the distribution of E_mE_n as a function of mode numbers m and n for six different values of N_{max}/N_0 and a fixed value for the normalized pycnocline thickness $h/\lambda_x = 1$ (thick pycnocline based on the terminology of Diamessis *et al.* (2014)). In each of figure 8(*a–c*), the distributions for two values of N_{max}/N_0 are shown as indicated within each figure. As shown in (2.16), the magnitude of h_{mn} is directly proportional to $\sqrt{E_mE_n}$; thus, it is relevant to look for only those resonant triads which contain modes m and n (at frequency ω) for which $\sqrt{E_mE_n}$ is non-negligible. Also shown as individual points (coloured pink and black) in figure 8 are the (m, n) combinations for which $|k^d|$ is less than 0.01 for the corresponding N_{max}/N_0. For $N_{max}/N_0 = 1.5$ (top left of figure 8*a*), the absence of any pink points indicates that there are no resonant triads containing modes m and n at frequency ω with non-negligible E_m and E_n. For $N_{max}/N_0 = 3$ (bottom right of figure 8*a*), $k^d \ll 1$ (black points) occurs at $(m, n) = (10, 10)$ (self-interaction) and $(m, n) = (25, 23)$, both of which imply the existence of resonant triads. The resonant triad containing $(m, n) = (25, 23)$ is potentially significant as the value of E_mE_n is appreciable, as indicated by the background colour. It is therefore expected that the higher harmonic waves are stronger for the case of $N_{max}/N_0 = 3$ in comparison to $N_{max}/N_0 = 1.5$. As we increase N_{max}/N_0 further (figure 8*b,c*), we observe an increase in the number of resonant triads within the region of non-negligible E_mE_n and therefore conclude that the amplitude of higher harmonics is likely to be larger for larger N_{max}/N_0 for a fixed value of $h/\lambda_x = 1$. This offers an explanation for one of the main observations of Diamessis *et al.* (2014), namely that the number and amplitude of higher harmonics increase with a stratification parameter defined as $\gamma = (N_{max}/N_0)/(h/\lambda_x)$. The precise number, amplitude and spatial pattern of higher harmonics would, however, require calculations of the energy transfer rates within the identified resonant triads, and also

a consideration of interactions that occur at higher frequencies. As a follow-up study, it would be intriguing to investigate the relation between stratification profiles that are conducive to solitary wave generation (Gerkema 2001) and those that correspond to the existence of a large number of resonant triads that contain the modes present in the incident wave beam.

5. Conclusions

In this paper, we have shown the existence of pure resonant triads in finite-depth non-uniform stratifications with background rotation. The weakly nonlinear solution corresponding to interaction between modes m and n in the linear solution comprises two different terms, one at frequency 2ω (horizontal wavenumber $k_m + k_n$ and vertical profile $\bar{h}_{mn}(z)$) and the other being time independent. The amplitude of the superharmonic term diverges if a resonance condition in the governing equation for $\bar{h}_{mn}(z)$ is met. The resonance condition is also interpreted as the existence of a resonant triad comprising modes m and n at frequency ω and the higher harmonic internal wave at frequency 2ω. The mode number q of the higher harmonic wave is $q = |m - n|$ for a uniform stratification, but seems to take some value less than $\max(m, n)$ for a non-uniform stratification with a pycnocline.

For a given modal pair (m, n), the resonance condition is satisfied along specific divergence curves on the $(\omega/N_0, f/\omega)$ plane in both uniform stratifications and ocean-like non-uniform stratifications. In uniform stratifications, a unique divergence curve exists for a given (m, n) that satisfies $(m/3) < n < 3m$. For the case of m/n close to unity, the divergence curves tend to become horizontal and accumulate close to $f/\omega \approx 1$. In non-uniform stratifications with a pycnocline, divergence curves occur for several more modal interactions than those for the uniform stratification; in fact, divergence curves occur for all $(m, n \neq m)$ we considered: $(m = 1,\ 2 \leqslant n \leqslant 7)$, $(m = 2,\ 3 \leqslant n \leqslant 5)$ and self-interactions too. Furthermore, multiple divergence curves occur for many (m, n) in non-uniform stratifications with a pycnocline, a significant consequence of which is an increase in the extent of the region on the $(\omega/N_0, f/\omega)$ plane where the higher harmonic solutions are of a large magnitude. For sufficiently strong pycnoclines, we observe the occurrence of near-horizontal divergence curves near $f/\omega \approx 1$ even for values of m/n far from unity, potentially a significant factor for understanding nonlinear effects in near-inertial waves. Remarkably, resonance occurs even for self-interaction $(m = n)$ in a non-uniform stratification, thus rendering the corresponding distinct modes at frequency ω unstable irrespective of their amplitude.

The divergence of the higher harmonic weakly nonlinear solution was shown to occur upon satisfying two different criteria: (i) $k_m + k_n = k_s^{2\omega}$, where $k_s^{2\omega}$ is the horizontal wavenumber of some mode-s at frequency 2ω, and (ii) the right-hand side $\bar{C}_{mn}(z)$ of the governing equation (2.18) of $\bar{h}_{mn}(z)$ should not be orthogonal to $Q_s^{2\omega}(z)$, where $Q_s^{2\omega}(z)$ is the vertical structure of mode-s at frequency 2ω. Criterion (i) is the same as the horizontal component of the standard triadic resonance criterion $\boldsymbol{k}_1 + \boldsymbol{k}_2 + \boldsymbol{k}_3 = 0$. For uniform stratifications, criterion (ii) coincides with the vertical component of $\boldsymbol{k}_1 + \boldsymbol{k}_2 + \boldsymbol{k}_3 = 0$, and is not necessarily satisfied upon satisfying criterion (i). In fact, there exist non-divergence curves on the $(\omega/N_0, f/\omega)$ plane along which criterion (i) but not criterion (ii) is satisfied for a uniform stratification. For non-uniform stratifications with a pycnocline, however, criterion (ii) was always satisfied upon the satisfaction of criterion (i) for all the cases we considered, and hence results in several more divergence curve/triadic resonance interactions than for a uniform stratification.

Two representative oceanic scenarios, namely low-mode internal tide scattering by topography and internal wave beam interaction with the pycnocline, were then discussed. In non-uniform stratifications with a pycnocline, mode-1 interaction with higher modes results in divergence curves over large portions of the $(\omega/N_0, f/\omega)$ plane, suggesting that RTIs are likely to occur over small-scale random topography in the ocean. The generation of higher harmonics upon the interaction of an internal wave beam with the pycnocline was then associated with the existence of resonant triads comprising two modes at frequency ω contained within the incident wave beam. Consistent with the numerical study of Diamessis *et al.* (2014), we were able to show that the number of resonant triads that result from interaction between the modes contained in a given incident wave beam increases with the maximum stratification in the pycnocline whose thickness is fixed.

The most significant contribution of our study is to demonstrate the existence of pure resonant triads in finite-depth non-uniform stratifications when the interaction between modes m and n is considered. The condition for resonant triad interaction involving modes m and n at frequency ω in both uniform and non-uniform stratifications is given by $k^d = k_m^\omega + k_n^\omega - k_q^{2\omega} = 0$, where the notation k_p^Ω stands for the horizontal wavenumber of mode-p at frequency Ω. Here, q is given by $q = n_z + 1$, where n_z is the number of zeros of the particular solution of the vertical structure $\bar{h}_{mn}(z)$ of the weakly nonlinear higher harmonic solution when a primary wave field containing modes m and n at frequency ω is assumed. It is noted that the particular solution of $\bar{h}_{mn}(z)$ diverges in the event of k^d being exactly zero. However, $k^d = 0$ is never exactly achieved in the numerical solutions, allowing us to build a finite-amplitude solution for $\bar{h}_{mn}(z)$ and hence calculate n_z. It is also noteworthy that numerical calculation of $\bar{h}_{mn}(z)$, as against adopting the graphical approach given in § 3.4, allows for a direct and efficient identification of triadic resonance/divergence curves on the entire $(\omega/N_0, f/\omega)$ plane. While our calculations were performed for idealized non-uniform stratifications, they can be readily extended to realistic ocean stratification profiles without making any assumptions about the pycnocline or the mixed layer characteristics. Finally, the inclusion of the effects of background rotation allowed us to discover phenomena that are potentially relevant for the dynamics of near-inertial waves.

The results in this paper could also represent a mechanism by which wind-generated near-inertial oscillations in the upper ocean get dissipated. Our study may help quantify the relative importance of the nonlinear energy transfer from near-inertial oscillations to other frequencies, in comparison to other mechanisms such as downward radiation of near-inertial waves (Young & Jelloul 1997) and turbulent dissipation (Hebert & Moum 1994). The tools presented in this paper can also be useful in the theoretical prediction of PSI and its characteristics in individual modes of a non-uniform stratification, a special case of which (primary wave frequency $\approx$ twice the inertial frequency) was studied by Young *et al.* (2008). Our ongoing efforts include a calculation of the amplitude evolution (and hence the growth rates) associated with the resonant triads identified in this paper and subsequent comparisons with direct numerical simulations. Finally, the influence of background shear, viscosity and three-dimensionality could be included to make our model even more relevant for realistic ocean settings.

Acknowledgements

The authors thank the Ministry of Earth Sciences, Government of India for financial support under the Monsoon Mission grant MM/2014/IND-002. The insightful comments from the three anonymous reviewers are gratefully acknowledged.

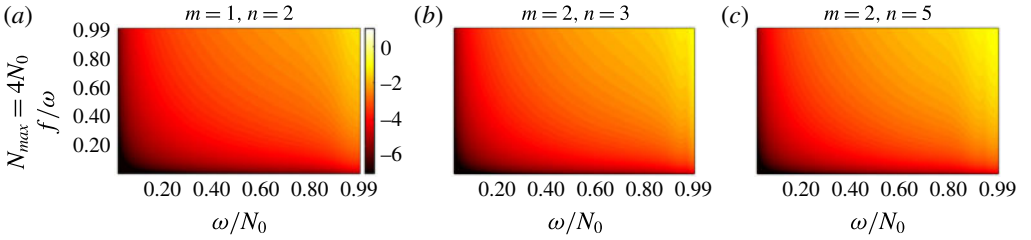

FIGURE 9. (Colour online) $\log_{10}[\bar{g}^{max}_{mn}]$ plotted as a function of ω/N_0 and f/ω for $(m, n) = (a)\ (1, 2)$, $(b)\ (2, 3)$ and $(c)\ (2, 5)$ with $N_{max} = 4N_0$. The energy fluxes for each plot are fixed at $(E_m, E_n) = (0.9, 0.1)$ W m^{-1}.

Appendix A. Mean flow in the weakly nonlinear solution

As shown in (3.2), the mean flow given by the time-independent term $\bar{g}_{mn}(z)$ does not diverge for any values of ω/N_0, f/ω, m and n in a uniform stratification. For a non-uniform stratification with $N_{max} = 4N_0$, we plot $\log_{10}[\bar{g}^{max}_{mn}]$ as a function of ω/N_0 and f/ω for three different modal pairs: $(m, n) = (1, 2), (2, 3), (2, 5)$ in figure 9(*a–c*), respectively. The mean flow again does not diverge anywhere on the $(\omega/N_0, f/\omega)$ plane, with $\log_{10}[\bar{g}^{max}_{mn}]$ increasing as a function of ω/N_0 and f/ω in most of the domain. There, however, exists a vertical line close to $(\omega/N_0) = 0.955$ along which $\log_{10}[\bar{g}^{max}_{mn}]$ attains a local minimum for $(m, n) = (2, 3)$ (figure 9*b*). For $(m, n) = (2, 5)$, as shown in figure 9(*c*), there again exists a local minimum along a vertical line, now occurring at $\omega/N_0 \approx 0.93$. We have furthermore verified via very fine-resolution (in ω/N_0) runs in the vicinity of the local maxima (that occur just to the left of the identified local minima) that there is no divergence of the mean flow in these regions of the parameter space.

Appendix B. Self-interactions in uniform stratification

The governing equation (2.18) for $\bar{h}_{mn}(z)$ reduces to

$$\frac{\mathrm{d}^2\bar{h}_{mm}}{\mathrm{d}z^2} + (2k_m)^2\frac{N_0^2 - (2\omega)^2}{(2\omega)^2 - f^2}\bar{h}_{mm} = 0 \tag{B 1}$$

for $n = m$ and a uniform stratification $N(z) = N_0$. Equation (B 1) is the well-known governing equation (2.12) for linear internal wave modes with horizontal wavenumber $2k_m$ and frequency 2ω. Therefore, non-zero solutions exist only if the vertical wavenumber $k_{z,2\omega}$ satisfies

$$k_{z,2\omega} = 2k_m\sqrt{\frac{N_0^2 - (2\omega)^2}{(2\omega)^2 - f^2}}, \tag{B 2}$$

with $k_{z,2\omega} = s\pi/H$ where the mode number s of the higher harmonic wave is a positive integer; s can now be written in terms of the mode number m of the primary wave as

$$s = 2m\sqrt{\frac{N_0^2 - (2\omega)^2}{(2\omega)^2 - f^2}}\sqrt{\frac{\omega^2 - f^2}{N_0^2 - \omega^2}}. \tag{B 3}$$

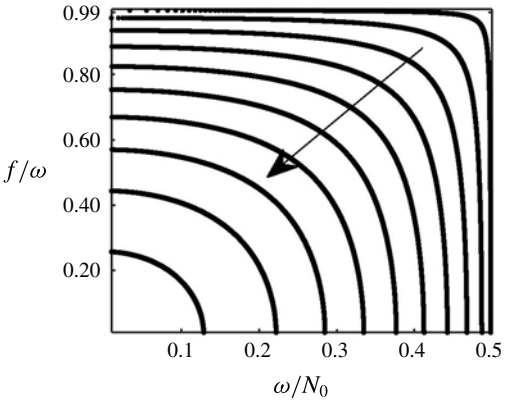

FIGURE 10. f/ω plotted as a function of ω/N_0 as given by (C 1) for resonant triads containing modes m and n to exist in a uniform stratification. The ten different curves correspond to increasing (in the direction of the arrow) equispaced values of m/n in the range $1.1 \leqslant (m/n) \leqslant 2.9$.

Non-zero solutions for $\bar{h}_{mm}(z)$ exist for all combinations of ω/N_0, f/ω and m that give an integer solution for s in (B 3). In the range $0 < (\omega/N_0) < 0.5$ and $0 < f/\omega < 1$, s can take any integer value in the range $1 \leqslant s < m$; each of these possible values of s occur along specific curves on the $(\omega/N_0, f/\omega)$ plane.

Appendix C. High-mode interactions in uniform stratification

Here, we plot (3.5) on the $(\omega/N_0, f/\omega)$ plane for all possible values of m/n that can result in the existence of resonant triads containing modes m and n at frequency ω. Equation (3.5) is rewritten as

$$\frac{\omega^2}{N_0^2} = \frac{(m/n+1)^2 - (m/n-1)^2(4 - f^2/\omega^2)/(1 - f^2/\omega^2)}{4(m/n+1)^2 - (m/n-1)^2(4 - f^2/\omega^2)/(1 - f^2/\omega^2)}. \tag{C 1}$$

As shown by condition (3.6) in § 3.1, m/n has to be in the range $(1/3) < (m/n) < 3$ for any divergence curve/resonant triad to exist on the $(\omega/N_0, f/\omega)$ plane. Since equation (C 1) is invariant with an interchange of m and n, we proceed to plot the divergence curves as f/ω versus ω/N_0 for the smaller range of $1 < (m/n) < 3$.

Figure 10 shows that for m/n close to 3, the divergence curve occurs for small values of ω/N_0 and f/ω. As m/n is decreased from 3, the divergence curve moves away from the origin, with the curve becoming near horizontal around $f/\omega \approx 1$ and near vertical around $\omega/N_0 \approx 0.5$ for m/n close to unity. With $m \neq n$, m/n close to unity is achieved only for relatively large values of m and n, i.e. high modes. Thus, we conclude that interaction between neighbouring high modes in a uniform stratification results in strong nonlinear effects in the near-inertial range, i.e. $(f/\omega) \approx 1$ for almost the entire range of $0 < (\omega/N_0) < 0.5$. It is worthwhile to recall that modes m and n at frequency ω generate mode $|m - n|$ at frequency 2ω, thereby implying that the corresponding resonant triad contains a low-mode higher harmonic at frequency 2ω and two high-mode waves at frequency ω.

One of the well-known mechanisms for low-mode tidal energy dissipation occurs via parametric subharmonic instability at around the critical latitude where

$(\omega_{M2}/2) \approx f$, with ω_{M2} and f being the semidiurnal frequency and the local Coriolis frequency, respectively (MacKinnon & Winters 2005). It was further shown in the numerical study of MacKinnon & Winters (2005) that the subharmonic waves at frequency $\omega_{M2}/2$ were of high modes whereas the primary wave is a low-mode semidiurnal tide. These results are consistent with our finding that two neighbouring high modes at a frequency ω and a low mode at frequency 2ω often form a resonant triad in the near-inertial range, i.e. $f/\omega \approx 1$ independent of the value of ω/N_0.

REFERENCES

Balmforth, N. J. & Young, W. R. 1999 Radiative damping of near-inertial oscillations in the mixed layer. *J. Mar. Res.* **57**, 561–584.

Bourget, B., Dauxois, T., Joubaud, S. & Odier, P. 2013 Experimental study of parametric subharmonic instability for internal plane waves. *J. Fluid Mech.* **723**, 1–20.

Bühler, O. & Holmes-Cerfon, M. 2011 Decay of an internal tide due to random topography in the ocean. *J. Fluid Mech.* **678**, 271–293.

Clark, H. A. & Sutherland, B. R. 2010 Generation, propagation, and breaking of an internal wave beam. *Phys. Fluids* **22**, 076601.

D'Asaro, E. A. 1989 The decay of wind-forced mixed layer inertial oscillations due to the β effect. *J. Geophys. Res.* **94** (C2), 2045–2056.

Diamessis, P. J., Wunsch, S., Delwiche, I. & Richter, M. P. 2014 Nonlinear generation of harmonics through the interaction of an internal wave beam with a model oceanic pycnocline. *Dyn. Atmos. Oceans* **66**, 110–137.

Garrett, C. & Kunze, E. 2007 Internal tide generation in the deep ocean. *Annu. Rev. Fluid Mech.* **39**, 57–87.

Gayen, B. & Sarkar, S. 2013 Degradation of an internal wave beam by parametric subharmonic instability in an upper ocean pycnocline. *J. Geophys. Res.* **118**, 4689–4698.

Gerkema, T. 2001 Internal and interfacial tides: beam scattering and local generation of solitary waves. *J. Mar. Res.* **59** (2), 227–255.

Ghaemsaidi, S. J., Joubaud, S., Dauxois, T., Odier, P. & Peacock, T. 2016 Nonlinear internal wave penetration via parametric subharmonic instability. *Phys. Fluids* **28**, 011703.

Gill, A. E. 1982 *Atmosphere-Ocean Dynamics*. Academic Press.

Grisouard, N., Staquet, C. & Gerkema, T. 2011 Generation of internal solitary waves in a pycnocline by an internal wave beam: a numerical study. *J. Fluid Mech.* **676**, 491–513.

Hasselmann, K. 1967 A criterion for nonlinear wave stability. *J. Fluid Mech.* **30** (04), 737–739.

Hebert, D. & Moum, J. N. 1994 Decay of a near-inertial wave. *J. Phys. Oceanogr.* **24** (11), 2334–2351.

Johnston, T. M. S., Merrifield, M. A. & Holloway, P. E. 2003 Internal tide scattering at the Line Islands Ridge. *J. Geophys. Res.* **108** (C11), 3365.

Joubaud, S., Munroe, J., Odier, P. & Dauxois, T. 2012 Experimental parametric subharmonic instability in stratified fluids. *Phys. Fluids* **24**, 041703.

Karimi, H. H. & Akylas, T. R. 2014 Parametric subharmonic instability of internal waves: locally confined beams versus monochromatic wavetrains. *J. Fluid Mech.* **757**, 381–402.

Klymak, J. M., Alford, M. H., Pinkel, R., Lien, R., Yang, Y. J. & Tang, T. 2011 The breaking and scattering of the internal tide on a continental slope. *J. Phys. Oceanogr.* **41** (5), 926–945.

Koudella, C. R. & Staquet, C. 2006 Instability mechanisms of a two-dimensional progressive internal gravity wave. *J. Fluid Mech.* **548**, 165–196.

LeBlond, P. H. & Mysak, L. A. 1981 *Waves in the Ocean*. Elsevier.

MacKinnon, J. A. & Winters, K. B. 2005 Subtropical catastrophe: significant loss of low-mode tidal energy at 28.9. *Geophys. Res. Lett.* **32** (15), L15605.

Martin, S., Simmons, W. & Wunsch, C. 1972 The excitation of resonant triads by single internal waves. *J. Fluid Mech.* **53** (01), 17–44.

MATHUR, M., CARTER, G. S. & PEACOCK, T. 2014 Topographic scattering of the low mode internal tide in the deep ocean. *J. Geophys. Res.* **119**, 2165–2182.

MERCIER, M., MATHUR, M., GOSTIAUX, L., GERKEMA, T., MAGALHAES, J. M., DA SILVA, J. C. B. & DAUXOIS, T. 2012 Soliton generation by internal tidal beams impinging on a pycnocline: laboratory experiments. *J. Fluid Mech.* **704**, 37–60.

MUNK, W. & WUNSCH, C. 1998 Abyssal recipes II: energetics of tidal and wind mixing. *Deep-Sea Res.* **45**, 1977–2010.

PEACOCK, T. & TABAEI, A. 2005 Visualization of nonlinear effects in reflecting internal wave beams. *Phys. Fluids* **17**, 061702.

STAQUET, C. & SOMMERIA, J. 2002 Internal gravity waves: from instabilities to turbulence. *Annu. Rev. Fluid Mech.* **34** (1), 559–593.

SUTHERLAND, B. R. 2016 Excitation of superharmonics by internal modes in non-uniformly stratified fluid. *J. Fluid Mech.* **793**, 335–352.

TABAEI, A. & AKYLAS, T. R. 2003 Nonlinear internal gravity wave beams. *J. Fluid Mech.* **482**, 141–161.

TABAEI, A., AKYLAS, T. R. & LAMB, K. G. 2005 Nonlinear effects in reflecting and colliding internal wave beams. *J. Fluid Mech.* **526**, 217–243.

THORPE, S. A. 1966 On wave interactions in a stratified fluid. *J. Fluid Mech.* **24** (04), 737–751.

THORPE, S. A. 1998 Nonlinear reflection of internal waves at a density discontinuity at the base of the mixed layer. *J. Phys. Oceanogr.* **28** (9), 1853–1860.

WUNSCH, S. 2015 Nonlinear harmonic generation by diurnal tides. *Dyn. Atmos. Oceans* **71**, 91–97.

WUNSCH, S. & BRANDT, A. 2012 Laboratory experiments on internal wave interactions with a pycnocline. *Exp. Fluids* **53** (6), 1663–1679.

WUNSCH, S., DELWICHE, I., FREDERICK, G. & BRANDT, A. 2015 Experimental study of nonlinear harmonic generation by internal waves incident on a pycnocline. *Exp. Fluids* **56** (5), 1–14.

WUNSCH, S., KU, H., DELWICHE, I. & AWADALLAH, R. 2014 Simulations of nonlinear harmonic generation by an internal wave beam incident on a pycnocline. *Nonlinear Process. Geophys.* **21** (4), 855–868.

XIE, X., SHANG, X., HAREN, H. & CHEN, G. 2013 Observations of enhanced nonlinear instability in the surface reflection of internal tides. *Geophys. Res. Lett.* **40** (8), 1580–1586.

YOUNG, W. R. & JELLOUL, M. B. 1997 Propagation of near-inertial oscillations through a geostrophic flow. *J. Mar. Res.* **55** (4), 735–766.

YOUNG, W. R., TSANG, Y.-K. & BALMFORTH, N. J. 2008 Near-inertial parametric subharmonic instability. *J. Fluid Mech.* **607**, 25–49.

ZHOU, Q. & DIAMESSIS, P. J. 2013 Reflection of an internal gravity wave beam off a horizontal free-slip surface. *Phys. Fluids* **25** (3), 036601.